II Neurons and Neural Circuits

This page intentionally left blank

5 Model Neurons I: Neuroelectronics

5.1 Introduction

A great deal is known about the biophysical mechanisms responsible for generating neuronal activity, and this knowledge provides a basis for constructing neuron models. Such models range from highly detailed descriptions involving thousands of coupled differential equations to greatly simplified caricatures useful for studying large interconnected networks. In this chapter, we discuss the basic electrical properties of neurons and the mathematical models by which they are described. We present a simple but nevertheless useful model neuron, the integrate-and-fire model, in a basic version and with added membrane and synaptic conductances. We also discuss the Hodgkin-Huxley model, which describes the conductances responsible for generating action potentials. In chapter 6, we continue by presenting more complex models, in terms of their conductances and morphology. Circuits and networks of model neurons are discussed in chapter 7. This chapter makes use of basic concepts of electrical circuit theory, which are reviewed in the Mathematical Appendix.

5.2 Electrical Properties of Neurons

Like other cells, neurons are packed with a huge number and variety of ions and molecules. A cubic micron of cytoplasm might contain, for example, 10^{10} water molecules, 10^8 ions, 10^7 small molecules such as amino acids and nucleotides, and 10^5 proteins. Many of these molecules carry charges, either positive or negative. Most of the time, there is an excess concentration of negative charge inside a neuron. Excess charges that are mobile, like ions, repel each other and build up on the inside surface of the cell membrane. Electrostatic forces attract an equal density of positive ions from the extracellular medium to the outside surface of the membrane.

cell membrane

The cell membrane is a lipid bilayer 3 to 4 nm thick that is essentially impermeable to most charged molecules. This insulating feature causes the cell membrane to act as a capacitor by separating the charges lying

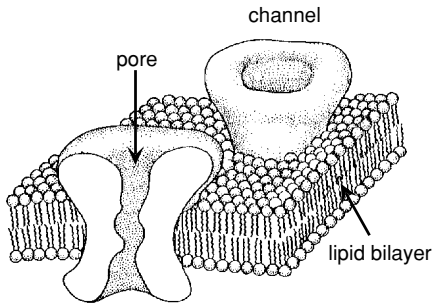

Figure 5.1 A schematic diagram of a section of the lipid bilayer that forms the cell membrane with two ion channels embedded in it. The membrane is 3 to 4 nm thick and the ion channels are about 10 nm long. (Adapted from Hille, 1992.)

ion channels

along its interior and exterior surfaces. Numerous ion-conducting channels embedded in the cell membrane (figure 5.1) lower the effective membrane resistance for ion flow to a value about 10,000 times smaller than that of a pure lipid bilayer. The resulting membrane conductance depends on the density and types of ion channels. A typical neuron may have a dozen or more different types of channels, anywhere from a few to hundreds of channels in a square micron of membrane, and hundreds of thousands to millions of channels in all. Many, but not all, channels are highly selective,

channel selectivity

allowing only a single type of ion to pass through them (to an accuracy of about 1 ion in 10^4). The capacity of channels for conducting ions across the cell membrane can be modified by many factors, including the membrane potential (voltage-dependent channels), the internal concentration of various intracellular messengers (Ca^{2+}-dependent channels, for example), and the extracellular concentration of neurotransmitters or neuromodulators (synaptic receptor channels, for example). The membrane also contains

ion pumps

selective pumps that expend energy to maintain differences in the concentrations of ions inside and outside the cell.

membrane potential

By convention, the potential of the extracellular fluid outside a neuron is defined to be 0. When a neuron is inactive, the excess internal negative charge causes the potential inside the cell membrane to be negative. This potential is an equilibrium point at which the flow of ions into the cell matches that out of the cell. The potential can change if the balance of ion flow is modified by the opening or closing of ion channels. Under normal conditions, neuronal membrane potentials vary over a range from about -90 to +50 mV. The order of magnitude of these potentials can be estimated from basic physical principles.

Membrane potentials are small enough to allow neurons to take advantage of thermal energy to help transport ions across the membrane, but are large enough so that thermal fluctuations do not swamp the signaling capabilities of the neuron. These conditions imply that potential differences across the cell membrane must lie in a range such that the energy gained or lost by an ion traversing the membrane is the same order of magnitude as its thermal energy. The thermal energy of an ion is about $k_B T$ where k_B

is the Boltzmann constant and T is the temperature on an absolute Kelvin scale. For chemists and biologists (though not for physicists), it is more customary to discuss moles of ions rather than single ions. A mole of ions has Avagadro's number times as much thermal energy as a single ion, or RT, where R is the universal gas constant, equal to 8.31 joules/mol K° = 1.99 cal/mol K°. RT is about 2500 joules/mol or 0.6 kCal/mol at normal temperatures.

To estimate the size of typical membrane potentials, we equate the thermal energy of a mole of ions to the energy gained or lost when a mole of ions crosses a membrane with a potential difference V_T across it. This energy is FV_T, where F is the Faraday constant, F = 96,480 coulombs/mol, equal to Avagadro's number times the charge of a single proton, q. Setting $FV_T = RT$ gives

V_T

$$V_T = \frac{RT}{F} = \frac{k_B T}{q}. \tag{5.1}$$

This is an important parameter that enters into a number of calculations. V_T is between 24 and 27 mV for the typical temperatures of cold- and warm-blooded animals. This sets the overall scale for membrane potentials across neuronal membranes, which range from about -3 to +2 times V_T.

Intracellular Resistance

Membrane potentials measured at different places within a neuron can take different values. For example, the potentials in the soma, dendrite, and axon can all be different. Potential differences between different parts of a neuron cause ions to flow within the cell, which tends to equalize these differences. The intracellular medium provides a resistance to such flow. This resistance is highest for long, narrow stretches of dendritic or axonal cable, such as the segment shown in figure 5.2. The longitudinal current I_L flowing along such a cable segment can be computed from Ohm's law. For the cylindrical segment of dendrite shown in figure 5.2, the longitudinal current flowing from right to left satisfies $V_2 - V_1 = I_L R_L$. Here, R_L is the longitudinal resistance, which grows in proportion to the length of the segment (long segments have higher resistances than short ones) and is inversely proportional to the cross-sectional area of the segment (thin segments have higher resistances than fat ones). The constant of proportionality, called the intracellular resistivity, r_L, typically falls in a range from 1 to 3 kΩ mm. The longitudinal resistance of the segment in figure 5.2 is r_L times the length L divided by the cross-sectional area πa^2, $R_L = r_L L/\pi a^2$. A segment 100 μm long with a radius of 2 μm has a longitudinal resistance of about 8 MΩ. A voltage difference of 8 mV would be required to force 1 nA of current down such a segment.

longitudinal current I_L

longitudinal resistance R_L

intracellular resistivity r_L

We can also use the intracellular resistivity to estimate crudely the conductance of a single channel. The conductance, being the inverse of a resistance, is equal to the cross-sectional area of the channel pore divided by

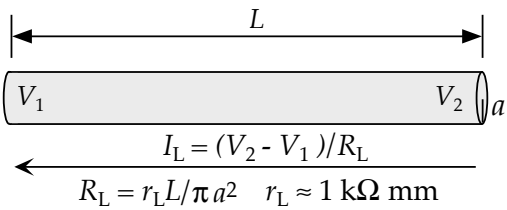

Figure 5.2 The longitudinal resistance of a cylindrical segment of neuronal cable with length L and radius a. The difference between the membrane potentials at the ends of this segment is related to the longitudinal current within the segment by Ohm's law, with R_L the longitudinal resistance of the segment. The arrow indicates the direction of positive current flow. The constant r_L is the intracellular resistivity, and a typical value is given.

its length and by r_L We approximate the channel pore as a tube of length 6 nm and opening area 0.15 nm^2. This gives an estimate of 0.15 nm^2/(1 kΩ mm × 6 nm) ≈ 25 pS, which is the right order of magnitude for a channel conductance.

single-channel conductance

Membrane Capacitance and Resistance

The intracellular resistance to current flow can cause substantial differences in the membrane potential measured in different parts of a neuron, especially during rapid transient excursions of the membrane potential from its resting value, such as action potentials. Neurons that have few of the long, narrow cable segments that produce high longitudinal resistances may have relatively uniform membrane potentials across their surfaces. Such neurons are termed electrotonically compact. For electrotonically compact neurons, or for less compact neurons in situations where spatial variations in the membrane potential are not thought to play an important functional role, the entire neuron may be adequately described by a single membrane potential. Here, we discuss the membrane capacitance and resistance using such a description. An analysis for the case of spatially varying membrane potentials is presented in chapter 6.

electrotonic compactness

We have mentioned that there is typically an excess negative charge on the inside surface of the cell membrane of a neuron, and a balancing positive charge on its outside surface (figure 5.3). In this arrangement, the cell membrane creates a capacitance C_m, and the voltage across the membrane V and the amount of this excess charge Q are related by the standard equation for a capacitor, $Q = C_m V$. The membrane capacitance is proportional to the total amount of membrane or, equivalently, to the surface area of the cell. The constant of proportionality, called the specific membrane capacitance, is the capacitance per unit area of membrane, and it is approximately the same for all neurons, $c_m \approx 10$ nF/mm^2. The total capacitance C_m is the membrane surface area A times the specific capacitance, $C_m = c_m A$. Neuronal surface areas tend to be in the range 0.01 to 0.1 mm^2, so the membrane capacitance for a whole neuron is typically 0.1

membrane capacitance C_m

specific membrane capacitance c_m

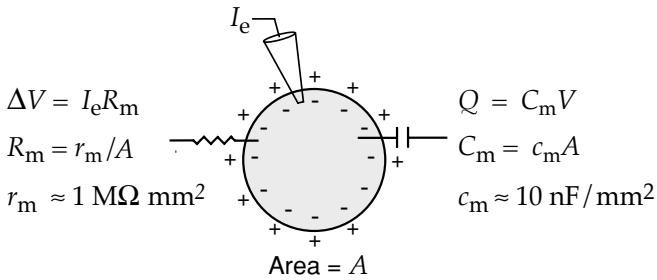

Figure 5.3 The capacitance and membrane resistance of a neuron considered as a single compartment. The membrane capacitance determines how the membrane potential V and excess internal charge Q are related. The membrane resistance R_m determines the size of the membrane potential deviation ΔV caused by a small current I_e entering through an electrode, for example. Equations relating the total membrane capacitance and resistance, C_m and R_m, to the specific membrane capacitance and resistance, c_m and r_m, are given along with typical values of c_m and r_m. The value of r_m may vary considerably under different conditions and for different neurons.

to 1 nF. For a neuron with a total membrane capacitance of 1 nF, 7×10^{-11} coulomb or about 10^9 singly charged ions are required to produce a resting potential of -70 mV. This is about 1/100,000 of the total number of ions in a neuron and is the amount of charge delivered by a 0.7 nA current in 100 ms.

We can use the membrane capacitance to determine how much current is required to change the membrane potential at a given rate. The time derivative of the basic equation relating the membrane potential and charge,

$$C_m \frac{dV}{dt} = \frac{dQ}{dt}, \tag{5.2}$$

plays an important role in the mathematical modeling of neurons. The time derivative of the charge dQ/dt is equal to the current passing into the cell, so the amount of current needed to change the membrane potential of a neuron with a total capacitance C_m at a rate dV/dt is $C_m dV/dt$. For example, 1 nA will change the membrane potential of a neuron with a capacitance of 1 nF at a rate of 1 mV/ms.

The capacitance of a neuron determines how much current is required to make the membrane potential change at a given rate. Holding the membrane potential steady at a level different from its resting value also requires current, but this current is determined by the membrane resistance rather than by the capacitance of the cell. For example, if a small constant current I_e is injected into a neuron through an electrode, as in figure 5.3, the membrane potential will shift away from its resting value by an amount ΔV given by Ohm's law, $\Delta V = I_e R_m$. R_m is known as the membrane or input resistance. The restriction to small currents and small ΔV is required because membrane resistances can vary as a function of voltage, whereas Ohm's law assumes R_m is constant over the range ΔV.

membrane resistance R_m

membrane conductance

specific membrane resistance r_m

The membrane resistance is the inverse of the membrane conductance, and, like the capacitance, the conductance of a piece of cell membrane is proportional to its surface area. The constant of proportionality is the membrane conductance per unit area, but we write it as $1/r_m$, where r_m is called the specific membrane resistance. Conversely, the membrane resistance R_m is equal to r_m divided by the surface area. When a neuron is in a resting state, the specific membrane resistance is around 1 MΩ mm^2. This number is much more variable than the specific membrane capacitance. Membrane resistances vary considerably among cells, and under different conditions and at different times for a given neuron, depending on the number, type, and state of its ion channels. For total surface areas between 0.01 and 0.1 mm, the membrane resistance is typically in the range 10 to 100 MΩ. With a 100 MΩ membrane resistance, a constant current of 0.1 nA is required to hold the membrane potential 10 mV away from its resting value.

membrane time constant τ_m

The product of the membrane capacitance and the membrane resistance is a quantity with the units of time called the membrane time constant, $\tau_m = R_m C_m$. Because C_m and R_m have inverse dependences on the membrane surface area, the membrane time constant is independent of area and equal to the product of the specific membrane capacitance and resistance, $\tau_m = r_m c_m$. The membrane time constant sets the basic time scale for changes in the membrane potential and typically falls in the range between 10 and 100 ms.

Equilibrium and Reversal Potentials

Electric forces and diffusion are responsible for driving ions through channel pores. Voltage differences between the exterior and interior of the cell produce forces on ions. Negative membrane potentials attract positive ions into the neuron and repel negative ions. In addition, ions diffuse through channels because the ion concentrations differ inside and outside the neuron. These differences are maintained by the ion pumps within the cell membrane. The concentrations of Na^+ and Ca^{2+} are higher outside the cell than inside, so these ions are driven into the neuron by diffusion. K^+ is more concentrated inside the neuron than outside, so it tends to diffuse out of the cell.

equilibrium potential

It is convenient to characterize the current flow due to diffusion in terms of an equilibrium potential. This is defined as the membrane potential at which current flow due to electric forces cancels the diffusive flow. For channels that conduct a single type of ion, the equilibrium potential can be computed easily. The potential difference across the cell membrane biases the flow of ions into or out of a neuron. Consider, for example, a positively charged ion and a negative membrane potential. In this case, the membrane potential opposes the flow of ions out of the the cell. Ions can cross the membrane and leave the interior of the cell only if they have sufficient thermal energy to overcome the energy barrier produced by the

membrane potential. If the ion has an electric charge zq, where q is the charge of one proton, it must have a thermal energy of at least $-zqV$ to cross the membrane (this is a positive energy for $z > 0$ and $V < 0$). The probability that an ion has a thermal energy greater than or equal to $-zqV$, when the temperature (on an absolute scale) is T, is $\exp(zqV/k_{\mathrm{B}}T)$. This is determined by integrating the Boltzmann distribution for energies greater than or equal to $-zqV$. In molar units, this result can be written as $\exp(zFV/RT)$, which is equal to $\exp(zV/V_T)$ by equation 5.1.

The biasing effect of the electrical potential can be overcome by an opposing concentration gradient. A concentration of ions inside the cell, [inside], that is sufficiently greater than the concentration outside the cell, [outside], can compensate for the Boltzmann probability factor. The rate at which ions flow into the cell is proportional to [outside]. The flow of ions out of the cell is proportional to [inside] times the Boltzmann factor, because in this direction only those ions that have sufficient thermal energy can leave the cell. The net flow of ions will be 0 when the inward and outward flows are equal. We use the letter E to denote the particular potential that satisfies this balancing condition, which is then

$$[\text{outside}] = [\text{inside}] \exp(zE/V_T) \,. \tag{5.3}$$

Solving this equation for E, we find *Nernst equation*

$$E = \frac{V_T}{z} \ln\left(\frac{[\text{outside}]}{[\text{inside}]}\right) . \tag{5.4}$$

Equation 5.4 is the Nernst equation. The reader can check that if the result is derived for either sign of ionic charge or membrane potential, the result is identical to 5.4, which thus applies in all cases. The equilibrium potential for a K^+ conducting channel, labeled E_{K}, typically falls in the range between -70 and -90 mV. The Na^+ equilibrium potential, E_{Na}, is 50 mV or higher, and E_{Ca}, for Ca^{2+} channels, is higher still, around 150 mV. Finally, Cl^- equilibrium potentials are typically around -60 to -65 mV, near the resting potential of many neurons.

The Nernst equation (5.4) applies when the channels that generate a particular conductance allow only one type of ion to pass through them. Some channels are not so selective, and in this case the potential E is not determined by equation 5.4. Instead, it takes a value intermediate between the equilibrium potentials of the individual ion types that it conducts. An approximate formula, known as the Goldman equation (see Tuckwell, 1988; or Johnston and Wu, 1995), can be used to estimate E for such conductances. In this case, E is often called a reversal potential, rather than an equilibrium potential, because the direction of current flow through the channel switches as the membrane potential passes through E. *Goldman equation* *reversal potential*

A conductance with an equilibrium or reversal potential E tends to move the membrane potential of the neuron toward the value E. When $V > E$, this means that positive current will flow outward, and when $V < E$, positive current will flow inward. Because Na^+ and Ca^{2+} conductances have

depolarization
hyperpolarization
shunting conductances
inhibitory and excitatory synapses

positive reversal potentials, they tend to depolarize a neuron (make its membrane potential less negative). K^+ conductances, with their negative E values, normally hyperpolarize a neuron (make its membrane potential more negative). Cl^- conductances, with reversal potentials near the resting potential, may pass little net current. Instead, their primary impact is to change the membrane resistance of the cell. Such conductances are sometimes called shunting, although all conductances "shunt", that is, increase the total conductance of a neuron. Synaptic conductances are also characterized by reversal potentials and are termed excitatory or inhibitory on this basis. Synapses with reversal potentials less than the threshold for action potential generation are typically called inhibitory, and those with reversal potentials above the action potential threshold are called excitatory.

The Membrane Current

The total current flowing across the membrane through all of its ion channels is called the membrane current of the neuron. By convention, the membrane current is defined as positive when positive ions leave the neuron and negative when positive ions enter the neuron. The total membrane current is determined by summing currents due to all of the different types of channels within the cell membrane, including voltage-dependent and synaptic channels. To facilitate comparisons between neurons of different sizes, it is convenient to use the membrane current per unit area of cell membrane, which we call i_m. The total membrane current is obtained from i_m by multiplying it by A, the total surface area of the cell.

membrane current per unit area i_m

We label the different types of channels in a cell membrane with an index i. As discussed in the last section, the current carried by a set of channels of type i with reversal potential E_i, vanishes when the membrane potential satisfies $V = E_i$. For many types of channels, the current increases or decreases approximately linearly when the membrane potential deviates from this value. The difference $V - E_i$ is called the driving force, and the membrane current per unit area due to the type i channels is written as $g_i(V - E_i)$. The factor g_i is the conductance per unit area, or specific conductance, due to these channels. Summing over the different types of channels, we obtain the total membrane current,

driving force
specific conductance g_i
membrane current

$$i_m = \sum_i g_i(V - E_i)\,. \tag{5.5}$$

Sometimes a more complicated expression called the Goldman-Hodgkin-Katz formula is used to relate the membrane current to g_i and membrane potential (see Tuckwell, 1988; or Johnston and Wu, 1995), but we will restrict our discussion to the simpler relationship used in equation 5.5.

Much of the complexity and richness of neuronal dynamics arises because membrane conductances change over time. However, some of the factors that contribute to the total membrane current can be treated as relatively constant, and these are typically grouped together into a single term

called the leakage current. The currents carried by ion pumps that maintain the concentration gradients that make equilibrium potentials nonzero typically fall into this category. For example, one type of pump uses the energy of ATP hydrolysis to move three Na^+ ions out of the cell for every two K^+ ions it moves in. *leakage current*

It is normally assumed that ion pumps work at relatively steady rates so that the currents they generate can be included in a time-independent leakage conductance. Sometimes, this assumption is dropped and explicit pump currents are modeled. In either case, all of the time-independent contributions to the membrane current can be lumped together into a single leakage term $\overline{g}_L(V - E_L)$. Because this term hides many sins, its reversal potential E_L is not usually equal to the equilibrium potential of any specific ion. Instead, it is often kept as a free parameter and adjusted to make the resting potential of the model neuron match that of the cell being modeled. Similarly, $\overline{g}_L$ is adjusted to match the membrane conductance at rest. The line over the parameter $\overline{g}_L$ is used to indicate that it has constant value. A similar notation is used later in this chapter to distinguish variable conductances from the fixed parameters that describe them. The leakage conductance is called a passive conductance to distinguish it from variable conductances that are termed active. *resting potential*

5.3 Single-Compartment Models

Models that describe the membrane potential of a neuron by a single variable V are called single-compartment models. This chapter deals exclusively with such models. Multi-compartment models, which can describe spatial variations in the membrane potential, are considered in chapter 6. The equations for single-compartment models, like those of all neuron models, describe how charges flow into and out of a neuron and affect its membrane potential.

Equation 5.2 provides the basic relationship that determines the membrane potential for a single-compartment model. This equation states that the rate of change of the membrane potential is proportional to the rate at which charge builds up inside the cell. The rate of charge buildup is, in turn, equal to the total amount of current entering the neuron. The relevant currents are those arising from all the membrane and synaptic conductances plus, in an experimental setting, any current injected into the cell through an electrode. From equation 5.2, the sum of these currents is equal to $C_m dV/dt$, the total capacitance of the neuron times the rate of change of the membrane potential. Because the membrane current is usually characterized as a current per unit area, i_m, it is more convenient to divide this relationship by the surface area of the neuron. Then, the total current per unit area is equal to $c_m dV/dt$, where $c_m = C_m/A$ is the specific membrane capacitance. One complication in this procedure is that the electrode current, I_e, is not typically expressed as a current per unit area, so we must divide it by the total surface area of the neuron, A. Putting all

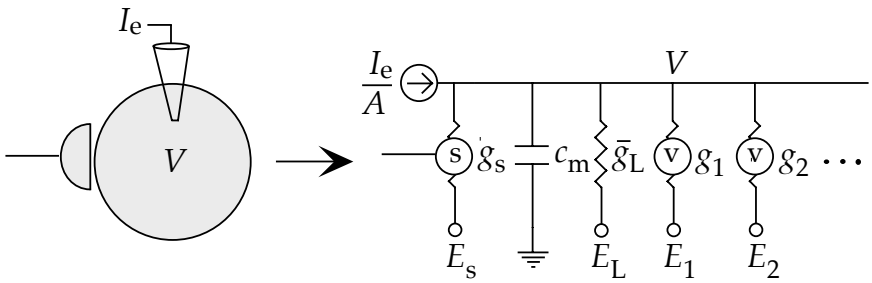

Figure 5.4 The equivalent circuit for a one-compartment neuron model. The neuron is represented, at the left, by a single compartment of surface area A with a synapse and a current-injecting electrode. At right is the equivalent circuit. The circled (S) indicates a synaptic conductance that depends on the activity of a presynaptic neuron. A single synaptic conductance g_s is indicated, but in general there may be several different types. The circled (V) indicates a voltage-dependent conductance, and I_e is the current passing through the electrode. The dots stand for possible additional membrane conductances.

this together, the basic equation for all single-compartment models is

$$c_m \frac{dV}{dt} = -i_m + \frac{I_e}{A}. \tag{5.6}$$

equivalent circuit

By convention, current that enters the neuron through an electrode is defined as positive-inward, whereas membrane current is defined as positive-outward. This explains the different signs for the currents in equation 5.6. The membrane current in equation 5.6 is determined by equation 5.5 and additional equations that specify the conductance variables g_i. The structure of such a model is the same as that of an electrical circuit, called the equivalent circuit, consisting of a capacitor and a set of variable and nonvariable resistors corresponding to the different membrane conductances. Figure 5.4 shows the equivalent circuit for a generic one-compartment model.

5.4 Integrate-and-Fire Models

A neuron will typically fire an action potential when its membrane potential reaches a threshold value of about -55 to -50 mV. During the action potential, the membrane potential follows a rapid, stereotyped trajectory and then returns to a value that is hyperpolarized relative to the threshold potential. As we will see, the mechanisms by which voltage-dependent K^+ and Na^+ conductances produce action potentials are well understood and can be modeled quite accurately. On the other hand, neuron models can be simplified and simulations can be accelerated dramatically if the biophysical mechanisms responsible for action potentials are not explicitly included in the model. Integrate-and-fire models do this by stipulating that an action potential occurs whenever the membrane potential of

the model neuron reaches a threshold value V_{th}. After the action potential, the potential is reset to a value V_{reset} below the threshold potential, $V_{\text{reset}} < V_{\text{th}}$.

The basic integrate-and-fire model was proposed by Lapicque in 1907, long before the mechanisms that generate action potentials were understood. Despite its age and simplicity, the integrate-and-fire model is still an extremely useful description of neuronal activity. By avoiding a biophysical description of the action potential, integrate-and-fire models are left with the simpler task of modeling only subthreshold membrane potential dynamics. This can be done with various levels of rigor. In the simplest version of these models, all active membrane conductances are ignored, including, for the moment, synaptic inputs, and the entire membrane conductance is modeled as a single passive leakage term, $i_{\text{m}} = \overline{g}_{\text{L}}(V - E_{\text{L}})$. This version is called the passive or leaky integrate-and-fire model. For small fluctuations about the resting membrane potential, neuronal conductances are approximately constant, and the passive integrate-and-fire model assumes that this constancy holds over the entire subthreshold range. For some neurons this is a reasonable approximation, and for others it is not. With these approximations, the model neuron behaves like an electric circuit consisting of a resistor and a capacitor in parallel (figure 5.4), and the membrane potential is determined by equation 5.6 with $i_{\text{m}} = \overline{g}_{\text{L}}(V - E_{\text{L}})$,

passive integrate-and-fire model

$$c_{\text{m}}\frac{dV}{dt} = -\overline{g}_{\text{L}}(V - E_{\text{L}}) + \frac{I_{\text{e}}}{A}. \tag{5.7}$$

It is convenient to multiply equation 5.7 by the specific membrane resistance r_{m}, which in this case is given by $r_{\text{m}} = 1/\overline{g}_{\text{L}}$. This cancels the factor of $\overline{g}_{\text{L}}$ on the right side of the equation and leaves a factor $c_{\text{m}}r_{\text{m}} = \tau_{\text{m}}$ on the left side, where τ_{m} is the membrane time constant of the neuron. The electrode current ends up being multiplied by r_{m}/A, which is the total membrane resistance R_{m}. Thus, the basic equation of the passive integrate-and-fire models is

$$\tau_{\text{m}}\frac{dV}{dt} = E_{\text{L}} - V + R_{\text{m}}I_{\text{e}}. \tag{5.8}$$

To generate action potentials in the model, equation 5.8 is augmented by the rule that whenever V reaches the threshold value V_{th}, an action potential is fired and the potential is reset to V_{reset}. Equation 5.8 indicates that when $I_{\text{e}} = 0$, the membrane potential relaxes exponentially with time constant τ_{m} to $V = E_{\text{L}}$. Thus, E_{L} is the resting potential of the model cell.

The membrane potential for the passive integrate-and-fire model is determined by integrating equation 5.8 (a numerical method for doing this is described in appendix A) and applying the threshold and reset rule for action potential generation. The response of a passive integrate-and-fire model neuron to a time-varying electrode current is shown in figure 5.5.

The firing rate of an integrate-and-fire model in response to a constant injected current can be computed analytically. When I_{e} is independent of

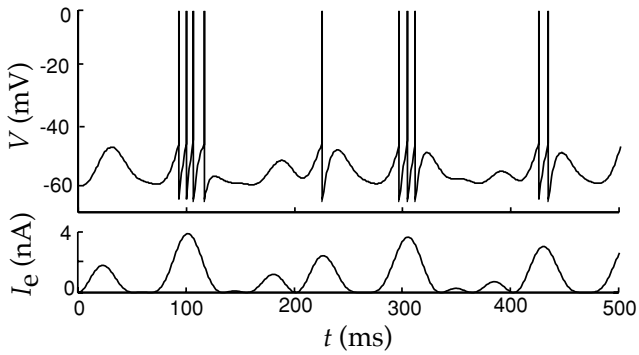

Figure 5.5 A passive integrate-and-fire model driven by a time-varying electrode current. The upper trace is the membrane potential, and the bottom trace the driving current. The action potentials in this figure are simply pasted onto the membrane potential trajectory whenever it reaches the threshold value. The parameters of the model are $E_L = V_{reset} = -65$ mV, $V_{th} = -50$ mV, $\tau_m = 10$ ms, and $R_m = 10$ MΩ.

time, the subthreshold potential $V(t)$ can easily be computed by solving equation 5.8, and is

$$V(t) = E_L + R_m I_e + (V(0) - E_L - R_m I_e) \exp(-t/\tau_m), \tag{5.9}$$

where $V(0)$ is the value of V at time $t = 0$. This solution can be checked by substituting it into equation 5.8. It is valid for the integrate-and-fire model only as long as V stays below the threshold. Suppose that at $t = 0$, the neuron has just fired an action potential and is thus at the reset potential, so that $V(0) = V_{reset}$. The next action potential will occur when the membrane potential reaches the threshold, that is, at a time $t = t_{isi}$ when

$$V(t_{isi}) = V_{th} = E_L + R_m I_e + (V_{reset} - E_L - R_m I_e) \exp(-t_{isi}/\tau_m). \tag{5.10}$$

By solving this for t_{isi}, the time of the next action potential, we can determine the interspike interval for constant I_e, or equivalently its inverse, which we call the interspike-interval firing rate of the neuron,

$$r_{isi} = \frac{1}{t_{isi}} = \left(\tau_m \ln\left(\frac{R_m I_e + E_L - V_{reset}}{R_m I_e + E_L - V_{th}}\right)\right)^{-1}. \tag{5.11}$$

This expression is valid if $R_m I_e > V_{th} - E_L$; otherwise $r_{isi} = 0$. For sufficiently large values of I_e, we can use the linear approximation of the logarithm ($\ln(1+z) \approx z$ for small z) to show that

$$r_{isi} \approx \left[\frac{E_L - V_{th} + R_m I_e}{\tau_m (V_{th} - V_{reset})}\right]_+, \tag{5.12}$$

which shows that the firing rate grows linearly with I_e for large I_e.

Figure 5.6A compares r_{isi} as a function of I_e, using appropriate parameter values, with data from current injection into a cortical neuron in vivo. The firing rate of the cortical neuron in figure 5.6A has been defined as the

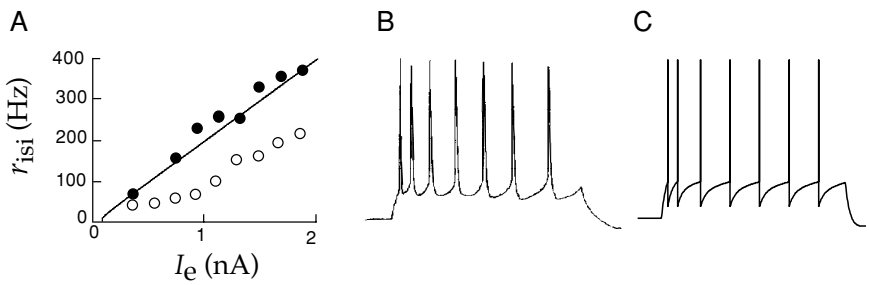

Figure 5.6 (A) Comparison of interspike-interval firing rates as a function of injected current for an integrate-and-fire model and a cortical neuron measure in vivo. The line gives r_{isi} for a model neuron with $\tau_m = 30$ ms, $E_L = V_{reset} = -65$ mV, $V_{th} = -50$ mV, and $R_m = 90$ MΩ. The data points are from a pyramidal cell in the primary visual cortex of a cat. The filled circles show the inverse of the interspike interval for the first two spikes fired, and the open circles show the steady-state interspike-interval firing rate after spike-rate adaptation. (B) A recording of the firing of a cortical neuron under constant current injection, showing spike-rate adaptation. (C) Membrane voltage trajectory and spikes for an integrate-and-fire model with an added current, with $r_m \Delta g_{sra} = 0.06$, $\tau_{sra} = 100$ ms, and $E_K = -70$ mV (see equations 5.13 and 5.14). (Data in A from Ahmed et al., 1998; B from McCormick, 1990.)

inverse of the interval between pairs of spikes. The rates determined in this way, using the first two spikes fired by the neuron in response to the injected current (filled circles in figure 5.6A), agree fairly well with the results of the integrate-and-fire model described in the figure caption. However, the real neuron exhibits spike-rate adaptation, in that the interspike intervals lengthen over time when a constant current is injected into the cell (figure 5.6B), before settling to a steady-state value. The steady-state firing rate in figure 5.6A (open circles) could also be fitted by an integrate-and-fire model, but not using the same parameters that were used to fit the initial spikes. Spike-rate adaptation is a common feature of cortical pyramidal cells, and consideration of this phenomenon allows us to show how an integrate-and-fire model can be modified to incorporate more complex dynamics.

spike-rate adaptation

Spike-Rate Adaptation and Refractoriness

The passive integrate-and-fire model that we have described thus far is based on two separate approximations, a highly simplified description of the action potential and a linear approximation for the total membrane current. If details of the action-potential generation process are not important for a particular modeling goal, the first approximation can be retained while the membrane current is modeled in as much detail as is necessary. We will illustrate this process by developing a heuristic description of spike-rate adaptation using a model conductance that has characteristics similar to measured neuronal conductances known to play important roles in producing this effect.

We model spike-rate adaptation by including an additional current in the model,

$$\tau_{\rm m}\frac{dV}{dt} = E_{\rm L} - V - r_{\rm m}g_{\rm sra}(V - E_K) + R_{\rm m}I_{\rm e}\,. \tag{5.13}$$

The spike-rate adaptation conductance $g_{\rm sra}$ has been modeled as a K^+ conductance so, when activated, it will hyperpolarize the neuron, slowing any spiking that may be occurring. We assume that this conductance relaxes to 0 exponentially with time constant $\tau_{\rm sra}$ through the equation

$$\tau_{\rm sra}\frac{dg_{\rm sra}}{dt} = -g_{\rm sra}\,. \tag{5.14}$$

Whenever the neuron fires a spike, $g_{\rm sra}$ is increased by an amount $\Delta g_{\rm sra}$, that is, $g_{\rm sra} \rightarrow g_{\rm sra} + \Delta g_{\rm sra}$. During repetitive firing, the current builds up in a sequence of steps causing the firing rate to adapt. Figures 5.6B and 5.6C compare the adapting firing pattern of a cortical neuron with the output of the model.

As discussed in chapter 1, the probability that a neuron fires is significantly reduced for a short period of time after the appearance of an action potential. Such a refractory effect is not included in the basic integrate-and-fire model. The simplest way of including an absolute refractory period in the model is to add a condition to the basic threshold crossing rule that forbids firing for a period of time immediately after a spike. Refractoriness can be incorporated in a more realistic way by adding a conductance similar to the spike-rate adaptation conductance discussed above, but with a faster recovery time and a larger conductance increment following an action potential. With a large increment, the current can essentially clamp the neuron to $E_{\rm K}$ following a spike, temporarily preventing further firing and producing an absolute refractory period. As this conductance relaxes back to 0, firing will be possible but initially less likely, producing a relative refractory period. When recovery is completed, normal firing can resume.

Another scheme that is sometimes used to model refractory effects is to raise the threshold for action-potential generation following a spike and then allow it to relax back to its normal value. Spike-rate adaptation can also be described by using an integrated version of the integrate-and-fire model known as the spike-response model, in which membrane potential waveforms are determined by summing precomputed postsynaptic potentials and after-spike hyperpolarizations. Finally, spike-rate adaptation and other effects can be incorporated into the integrate-and-fire framework by allowing the parameters $\overline{g}_{\rm L}$ and $E_{\rm L}$ in equation 5.7 to vary with time.

5.5 Voltage-Dependent Conductances

Most of the interesting electrical properties of neurons, including their ability to fire and propagate action potentials, arise from nonlinearities

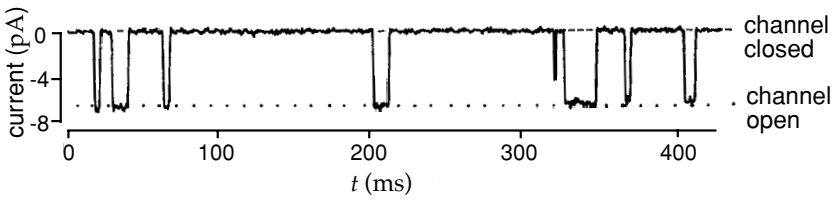

Figure 5.7 Recording of the current passing through a single ion channel. This is a synaptic receptor channel sensitive to the neurotransmitter acetylcholine. A small amount of acetylcholine was applied to the preparation to produce occasional channel openings. In the open state, the channel passes 6.6 pA at a holding potential of -140 mV. This is equivalent to more than 10^7 charges per second passing through the channel, and corresponds to an open channel conductance of 47 pS. (From Hille, 1992.)

associated with active membrane conductances. Recordings of the current flowing through single channels indicate that channels fluctuate rapidly between open and closed states in a stochastic manner (figure 5.7). Models of membrane and synaptic conductances must describe how the probability that a channel is in an open, ion-conducting state at any given time depends on the membrane potential (for a voltage-dependent conductance), the presence or absence of a neurotransmitter (for a synaptic conductance), or a number of other factors, such as the concentration of Ca^{2+} or other messenger molecules inside the cell. In this chapter, we consider two classes of active conductances, voltage-dependent membrane conductances and transmitter-dependent synaptic conductances. An additional type, the Ca^{2+}-dependent conductance, is considered in chapter 6.

stochastic channel

voltage-dependent, synaptic, and Ca^{2+}-dependent conductances

In a later section of this chapter, we discuss stochastic models of individual channels based on state diagrams and transition rates. However, most neuron models use deterministic descriptions of the conductances arising from many channels of a given type. This is justified because of the large number of channels of each type in the cell membrane of a typical neuron. If large numbers of channels are present, and if they fluctuate independently of each other (which they do, to a good approximation), then, from the law of large numbers, the fraction of channels open at any given time is approximately equal to the probability that any one channel is in an open state. This allows us to move between single-channel probabilistic formulations and macroscopic deterministic descriptions of membrane conductances.

We have denoted the conductance per unit area of membrane due to a set of ion channels of type i by g_i. The value of g_i at any given time is determined by multiplying the conductance of an open channel by the density of channels in the membrane and by the fraction of channels that are open at that time. The product of the first two factors is a constant called the maximal conductance that is denoted by $\overline{g}_i$. It is the conductance per unit area of membrane if all the channels of type i are open. Maximal conductance parameters tend to range from $\mu S/mm^2$ to mS/mm^2. The fraction of channels in the open state is equivalent to the probability of finding any

open probability P_i

given channel in the open state, and it is denoted by P_i. Thus, $g_i = \overline{g}_i P_i$. The dependence of a conductance on voltage, transmitter concentration, or other factors arises through effects on the open probability.

The open probability of a voltage-dependent conductance depends, as its name suggests, on the membrane potential of the neuron. In this chapter, we discuss models of two such conductances, the so-called delayed-rectifier K^+ and fast Na^+ conductances. The formalism we present, which is almost universally used to describe voltage-dependent conductances, was developed by Hodgkin and Huxley (1952) as part of their pioneering work showing how these conductances generate action potentials in the squid giant axon. Other conductances are modeled in chapter 6.

Persistent Conductances

Figure 5.8 shows cartoons of the mechanisms by which voltage-dependent channels open and close as a function of membrane potential. Channels are depicted for two different types of conductances, termed persistent (figure 5.8A) and transient (figure 5.8B). We begin by discussing persistent conductances. Figure 5.8A shows a swinging gate attached to a voltage sensor that can open or close the pore of the channel. In reality, channel gating mechanisms involve complex changes in the conformational structure of the channel, but the simple swinging gate picture is sufficient if we are interested only in the current-carrying capacity of the channel. A channel that acts as if it had a single type of gate (although, as we will see, this is actually modeled as a number of identical subgates), like the channel in figure 5.8A, produces what is called a persistent or noninactivating conductance. Opening of the gate is called activation of the conductance, and gate closing is called deactivation. For this type of channel, the probability that the gate is open, P_K, increases when the neuron is depolarized and decreases when it is hyperpolarized. The delayed-rectifier K^+ conductance that is responsible for repolarizing a neuron after an action potential is such a persistent conductance.

channel gate

activation
deactivation

The opening of the gate that describes a persistent conductance may involve a number of conformational changes. For example, the delayed-rectifier K^+ conductance is constructed from four identical subunits, and it appears that all four must undergo a structural change for the channel to open. In general, if k independent, identical events are required for a channel to open, P_K can be written as

$$P_K = n^k , \tag{5.15}$$

where n is the probability that any one of the k independent gating events has occurred. Here, n, which varies between 0 and 1, is called a gating or an activation variable, and a description of its voltage and time dependence amounts to a description of the conductance. We can think of n as the probability of an individual subunit gate being open, and $1 - n$ as the probability that it is closed.

activation variable n

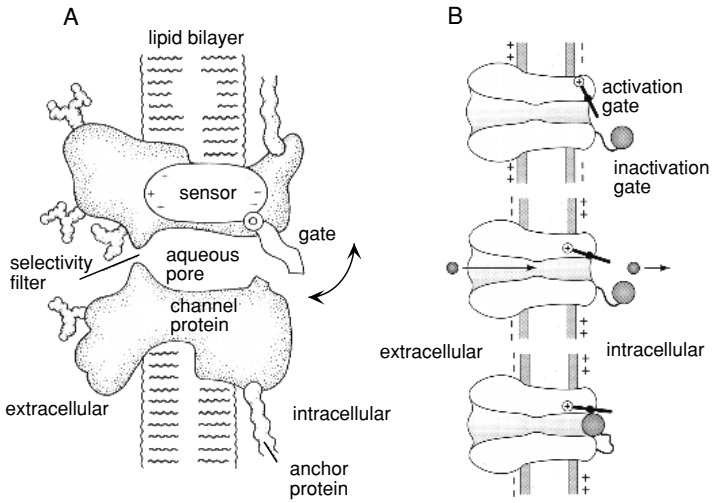

Figure 5.8 Gating of membrane channels. In both figures, the interior of the neuron is to the right of the membrane, and the extracellular medium is to the left. (A) A cartoon of gating of a persistent conductance. A gate is opened and closed by a sensor that responds to the membrane potential. The channel also has a region that selectively allows ions of a particular type to pass through the channel, for example, K^+ ions for a potassium channel. (B) A cartoon of the gating of a transient conductance. The activation gate is coupled to a voltage sensor (denoted by a circled +) and acts like the gate in A. A second gate, denoted by the ball, can block that channel once it is open. The top figure shows the channel in a deactivated (and deinactivated) state. The middle panel shows an activated channel, and the bottom panel shows an inactivated channel. Only the middle panel corresponds to an open, ion-conducting state. (A from Hille, 1992; B from Kandel et al., 1991.)

Although using the value of $k = 4$ is consistent with the four-subunit structure of the delayed-rectifier conductance, in practice k is an integer chosen to fit the data, and should be interpreted as a functional definition of a subunit rather than a reflection of a realistic structural model of the channel. Indeed, the structure of the channel was not known at the time that Hodgkin and Huxley chose the form of equation 5.15 and suggested that $k = 4$.

channel kinetics

We describe the transition of each subunit gate by a simple kinetic scheme in which the gating transition closed $\rightarrow$ open occurs at a voltage-dependent rate $\alpha_n(V)$, and the reverse transition, open $\rightarrow$ closed, occurs at a voltage-dependent rate $\beta_n(V)$. The probability that a subunit gate opens over a short interval of time is proportional to the probability of finding the gate closed, $1 - n$, multiplied by the opening rate $\alpha_n(V)$. Likewise, the probability that a subunit gate closes during a short time interval is proportional to the probability of finding the gate open, n, multiplied by the closing rate $\beta_n(V)$. The rate at which the open probability for a subunit gate changes is given by the difference of these two terms,

opening rate $\alpha_n(V)$

closing rate $\beta_n(V)$

$$\frac{dn}{dt} = \alpha_n(V)(1 - n) - \beta_n(V)n\,. \tag{5.16}$$

The first term in equation 5.16 describes the opening process, and the second term the closing process (hence the minus sign) that lowers the probability of being in the configuration with an open subunit gate. Equation 5.16 can be written in another useful form by dividing through by $\alpha_n(V) + \beta_n(V)$,

gating equation

$$\tau_n(V)\frac{dn}{dt} = n_\infty(V) - n\,, \tag{5.17}$$

$\tau_n(V)$

where

$$\tau_n(V) = \frac{1}{\alpha_n(V) + \beta_n(V)} \tag{5.18}$$

$n_\infty(V)$

and

$$n_\infty(V) = \frac{\alpha_n(V)}{\alpha_n(V) + \beta_n(V)}. \tag{5.19}$$

Equation 5.17 indicates that for a fixed voltage V, n approaches the limiting value $n_\infty(V)$ exponentially with time constant $\tau_n(V)$.

The key elements in the equation that determines n are the opening and closing rate functions $\alpha_n(V)$ and $\beta_n(V)$. These are obtained by fitting experimental data. It is useful to discuss the form that we expect these rate functions to take on the basis of thermodynamic arguments. The state transitions described by α_n, for example, are likely to be rate-limited by barriers requiring thermal energy. These transitions involve the movement of charged components of the gate across part of the membrane, so the height of these energy barriers should be affected by the membrane potential. The transition requires the movement of an effective charge, which we denote by qB_α, through the potential V. This requires an energy $qB_\alpha V$. The constant B_α reflects both the amount of charge being moved and the distance over which it travels. The probability that thermal fluctuations will provide enough energy to surmount this energy barrier is proportional to the Boltzmann factor, $\exp(-qB_\alpha V/k_\mathrm{B}T)$. Based on this argument, we expect α_n to be of the form

$$\alpha_n(V) = A_\alpha \exp(-qB_\alpha/k_\mathrm{B}T) = A_\alpha \exp(-B_\alpha V/V_T) \tag{5.20}$$

for some constant A_α. The closing rate β_n should be expressed similarly, except with different constants A_β and B_β. From equation 5.19, we then find that $n_\infty(V)$ is expected to be a sigmoidal function

$$n_\infty(V) = \frac{1}{1 + (A_\beta/A_\alpha)\exp((B_\alpha - B_\beta)V/V_T)}\,. \tag{5.21}$$

For a voltage-activated conductance, depolarization causes n to grow toward 1, and hyperpolarization causes n to shrink toward 0. Thus, we expect that the opening rate, α_n, should be an increasing function of V (and thus $B_\alpha < 0$), and β_n should be a decreasing function of V (and thus $B_\beta > 0$). Examples of the functions we have discussed are plotted in figure 5.9.

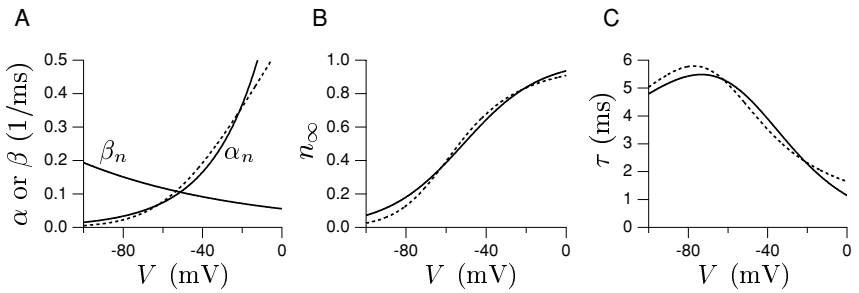

Figure 5.9 Generic voltage-dependent gating functions compared with Hodgkin-Huxley results for the delayed-rectifier K^+ conductance. (A) The exponential α_n and β_n functions expected from thermodynamic arguments are indicated by the solid curves. Parameter values used were $A_\alpha = 1.22$ ms^{-1}, $A_\beta = 0.056$ ms^{-1}, $B_\alpha/V_T = -0.04$/mV, and $B_\beta/V_T = 0.0125$/mV. The fit of Hodgkin and Huxley for β_n is identical to the solid curve shown. The Hodgkin-Huxley fit for α_n is the dashed curve. (B) The corresponding function $n_\infty(V)$ of equation 5.21 (solid curve). The dashed curve is obtained using the α_n and β_n functions of the Hodgkin-Huxley fit (equation 5.22). (C) The corresponding function $\tau_n(V)$, obtained from equation 5.18 (solid curve). Again the dashed curve is the result of using the Hodgkin-Huxley rate functions.

While thermodynamic arguments support the forms we have presented, they rely on simplistic assumptions. Not surprisingly, the resulting functional forms do not always fit the data, and various alternatives are often employed. The data upon which these fits are based are typically obtained using a technique called voltage clamping. In this technique, an amplifier is configured to inject the appropriate amount of electrode current to hold the membrane potential at a constant value. By current conservation, this current is equal to the membrane current of the cell. Hodgkin and Huxley fitted the rate functions for the delayed-rectifier K^+ conductance they studied, using the equations

voltage clamping

$$\alpha_n = \frac{.01(V+55)}{1-\exp(-.1(V+55))} \quad \text{and} \quad \beta_n = 0.125\exp(-0.0125(V+65))\,, \tag{5.22}$$

where V is expressed in mV, and α_n and β_n are both expressed in units of 1/ms. The fit for β_n is exactly the exponential form we have discussed, with $A_\beta = 0.125\exp(-0.0125\cdot 65)$ ms^{-1} and $B_\beta/V_T = 0.0125$ mV^{-1}, but the fit for α_n uses a different functional form. The dashed curves in figure 5.9 plot the formulas of equation 5.22.

Transient Conductances

Some channels only open transiently when the membrane potential is depolarized because they are gated by two processes with opposite voltage dependences. Figure 5.8B is a schematic of a channel that is controlled by two gates and generates a transient conductance. The swinging gate in figure 5.8B behaves exactly like the gate in figure 5.8A. The probability that it

activation variable m

is open is written as m^k, where m is an activation variable similar to n and k is an integer. Hodgkin and Huxley used $k = 3$ for their model of the fast Na^+ conductance. The ball in figure 5.8B acts as the second gate. The probability that the ball does not block the channel pore is written as h and is called the inactivation variable. The activation and inactivation variables m and h are distinguished by having opposite voltage dependences. Depolarization causes m to increase and h to decrease, and hyperpolarization decreases m while increasing h.

inactivation variable h

For the channel in figure 5.8B to conduct, both gates must be open, and assuming the two gates act independently, this has probability

$$P_{\mathrm{Na}} = m^k h\,. \tag{5.23}$$

This is the general form used to describe the open probability for a transient conductance. We could raise the h factor in this expression to an arbitrary power, as we did for m, but we omit this complication to streamline the discussion. The activation m and inactivation h, like all gating variables, vary between 0 and 1. They are described by equations identical to 5.16, except that the rate functions α_n and β_n are replaced by either α_m and β_m, or α_h and β_h. These rate functions were fitted by Hodgkin and Huxley using the equations (in units of 1/ms with V in mV)

$$\begin{aligned} \alpha_m &= \frac{.1(V+40)}{1-\exp(-.1(V+40))} & \beta_m &= 4\exp(-.0556(V+65)) \\ \alpha_h &= .07\exp(-.05(V+65)) & \beta_h &= 1/(1+\exp(-.1(V+35)))\,. \end{aligned} \tag{5.24}$$

Functions $m_\infty(V)$ and $h_\infty(V)$ describing the steady-state activation and inactivation levels, and voltage-dependent time constants for m and h can be defined as in equations 5.19 and 5.18. These are plotted in figure 5.10. For comparison, $n_\infty(V)$ and $\tau_n(V)$ for the K^+ conductance are also plotted. Note that $h_\infty(V)$, because it corresponds to an inactivation variable, is flipped relative to $m_\infty(V)$ and $n_\infty(V)$, so that it approaches 1 at hyperpolarized voltages and 0 at depolarized voltages.

The presence of two factors in equation (5.23) gives a transient conductance some interesting properties. To turn on a transient conductance maximally, it may first be necessary to hyperpolarize the neuron below its resting potential and then to depolarize it. Hyperpolarization raises the value of the inactivation h, a process called deinactivation. The second step, depolarization, increases the value of m, which is activation. Only when m and h are both nonzero is the conductance turned on. Note that the conductance can be reduced in magnitude by either decreasing m or h. Decreasing h is called inactivation to distinguish it from decreasing m, which is deactivation.

deinactivation

inactivation

Hyperpolarization-Activated Conductances

Persistent currents act as if they are controlled by an activation gate, while transient currents act as if they have both an activation and an inactivation

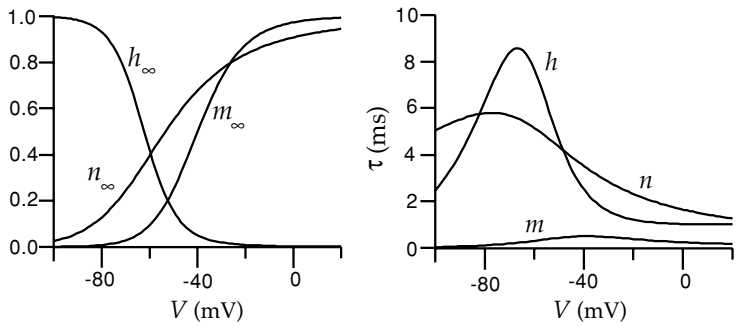

Figure 5.10 The voltage-dependent functions of the Hodgkin-Huxley model. The left panel shows $m_\infty(V)$, $h_\infty(V)$, and $n_\infty(V)$, the steady-state levels of activation and inactivation of the Na^+ conductance, and activation of the K^+ conductance. The right panel shows the voltage-dependent time constants that control the rates at which these steady-state levels are approached for the three gating variables.

gate. Another class of conductances, the hyperpolarization-activated conductances, behave as if they are controlled solely by an inactivation gate. They are thus persistent conductances, but they open when the neuron is hyperpolarized rather than depolarized. The opening probability for such channels is written solely in terms of an inactivation variable similar to h. Strictly speaking, these conductances deinactivate when they turn on and inactivate when they turn off. However, most people cannot bring themselves to say "deinactivate" all the time, so they say instead that these conductances are activated by hyperpolarization.

5.6 The Hodgkin-Huxley Model

The Hodgkin-Huxley model for the generation of the action potential, in its single-compartment form, is constructed by writing the membrane current in equation 5.6 as the sum of a leakage current, a delayed-rectified K^+ current, and a transient Na^+ current,

$$i_m = \overline{g}_L(V - E_L) + \overline{g}_K n^4(V - E_K) + \overline{g}_{Na} m^3 h(V - E_{Na}) . \qquad (5.25)$$

The maximal conductances and reversal potentials used in the model are $\overline{g}_L = 0.003$ mS/mm^2, $\overline{g}_K = 0.36$ mS/mm^2, $\overline{g}_{Na} = 1.2$ mS/mm^2, E_L = -54.387 mV, E_K = -77 mV and $E_{Na} = 50$ mV. The full model consists of equation 5.6 with equation 5.25 for the membrane current, and equations of the form 5.17 for the gating variables n, m, and h. These equations can be integrated numerically, using the methods described in appendices A and B.

The temporal evolution of the dynamic variables of the Hodgkin-Huxley model during a single action potential is shown in figure 5.11. The initial rise of the membrane potential, prior to the action potential, seen in the upper panel of figure 5.11, is due to the injection of a positive electrode current into the model starting at $t = 5$ ms. When this current drives the

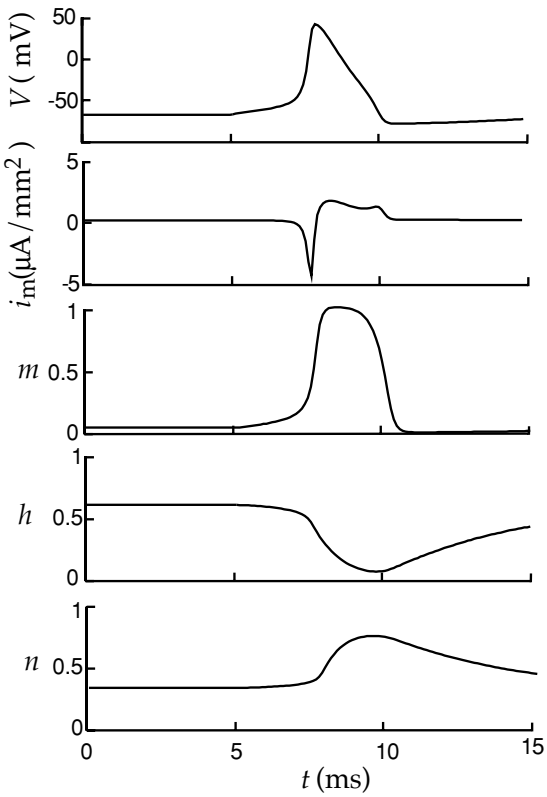

Figure 5.11 The dynamics of V, m, h, and n in the Hodgkin-Huxley model during the firing of an action potential. The upper-most trace is the membrane potential, the second trace is the membrane current produced by the sum of the Hodgkin-Huxley K^+ and Na^+ conductances, and subsequent traces show the temporal evolution of m, h, and n. Current injection was initiated at $t = 5$ ms.

membrane potential up to about about -50 mV, the m variable that describes activation of the Na^+ conductance suddenly jumps from nearly 0 to a value near 1. Initially, the h variable, expressing the degree of inactivation of the Na^+ conductance, is around 0.6. Thus, for a brief period both m and h are significantly different from 0. This causes a large influx of Na^+ ions, producing the sharp downward spike of inward current shown in the second trace from the top. The inward current pulse causes the membrane potential to rise rapidly to around 50 mV (near the Na^+ equilibrium potential). The rapid increase in both V and m is due to a positive feedback effect. Depolarization of the membrane potential causes m to increase, and the resulting activation of the Na^+ conductance makes V increase. The rise in the membrane potential causes the Na^+ conductance to inactivate by driving h toward 0. This shuts off the Na^+ current. In addition, the rise in V activates the K^+ conductance by driving n toward 1. This increases the K^+ current, which drives the membrane potential back down to negative values. The final recovery involves the readjustment of m, h, and n to their initial values.

The Hodgkin-Huxley model can also be used to study propagation of an action potential down an axon, but for this purpose a multi-compartment model must be constructed. Methods for building such a model, and results from it, are described in chapter 6.

5.7 Modeling Channels

In previous sections, we described the Hodgkin-Huxley formalism for describing voltage-dependent conductances arising from a large number of channels. With the advent of single-channel studies, microscopic descriptions of the transitions between the conformational states of channel molecules have been developed. Because these models describe complex molecules, they typically involve many states and transitions. Here, we discuss simple versions of these models that capture the spirit of single-channel modeling without getting mired in the details.

Models of single channels are based on state diagrams that indicate the possible conformational states that the channel can assume. Typically, one of the states in the diagram is designated as open and ion-conducting, while the other states are nonconducting. The current conducted by the channel is written as $\overline{g}P(V - E)$, where E is the reversal potential, $\overline{g}$ is the single-channel open conductance, and P is 1 whenever the open state is occupied, and 0 otherwise. Channel models can be instantiated directly from state diagrams simply by keeping track of the state of the channel and allowing stochastic changes of state to occur at appropriate transition rates. If the model is updated in short time steps of duration Δt, the probability that the channel makes a given transition during an update interval is the transition rate times Δt.

Figure 5.12 shows the state diagram and simulation results for a model of a single delayed-rectifier K^+ channel that is closely related to the Hodgkin-Huxley description of the macroscopic delayed-rectifier conductance. The factors α_n and β_n in the transition rates shown in the state diagram of figure 5.12 are the voltage-dependent rate functions of the Hodgkin-Huxley model. The model uses the same four subunit structure assumed in the Hodgkin-Huxley model. We can think of state 1 in this diagram as a state in which all the subunit gates are closed. States 2, 3, 4, and 5 have 1, 2, 3, and 4 open subunit gates, respectively. State 5 is the sole open state. The factors of 1, 2, 3, and 4 in the transition rates in figure 5.12 correspond to the number of subunit gates that can make a given transition. For example, the transition rate from state 1 to state 2 is four times faster than the rate from state 4 to state 5. This is because any one of the four subunit gates can open to get from state 1 to state 2, but the transition from state 4 to state 5 requires the single remaining closed subunit gate to open.

The lower panels in figure 5.12 show simulations of this model involving 1, 10, and 100 channels. The sum of currents from all of these channels is compared with the current predicted by the Hodgkin-Huxley model

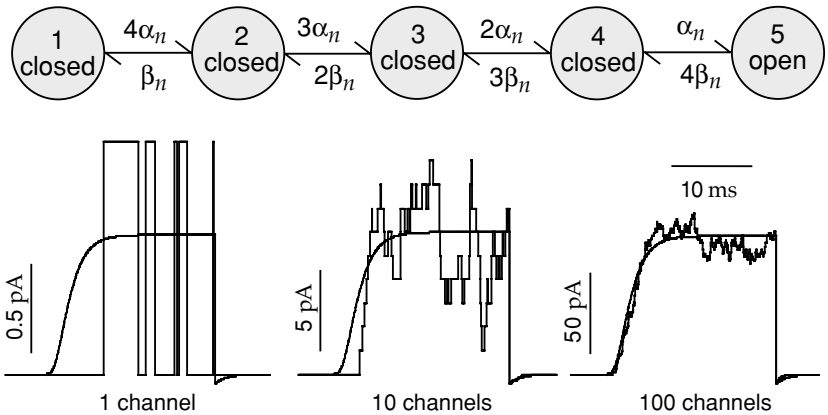

Figure 5.12 A model of the delayed-rectifier K^+ channel. The upper diagram shows the states and transition rates of the model. In the simulations shown in the lower panels, the membrane potential was initially held at -100 mV, then held at 10 mV for 20 ms, and finally returned to a holding potential of -100 mV. The smooth curves in these panels show the membrane current predicted by the Hodgkin-Huxley model in this situation. The left panel shows a simulation of a single channel that opened several times during the depolarization. The middle panel shows the total current from 10 simulated channels, and the right panel corresponds to 100 channels. As the number of channels increases, the Hodgkin-Huxley model provides a more accurate description of the current.

(scaled by the appropriate maximal conductance). For each channel, the pattern of opening and closing is random, but when enough channels are summed, the total current matches that of the Hodgkin-Huxley model quite well.

To see how the channel model in figure 5.12 reproduces the results of the Hodgkin-Huxley model when the currents from many channels are summed, we must consider a probabilistic description of the channel model. We denote the probability that a channel is in state a of figure 5.12 by p_a, with $a = 1, 2, \ldots, 5$. Dynamic equations for these probabilities are easily derived by setting the rate of change for a given p_a equal to the probability per unit time of entry into state a from other states minus the rate for leaving state a. The entry probability per unit time is the product of the appropriate transition rate times the probability that the state making the transition is occupied. The probability per unit time for leaving is p_a times the sum of all the rates for possible transitions out of the state. Following this reasoning, the equations for the state probabilities are (using the notation $\dot{p} = dp/dt$)

$$\begin{aligned}
\dot{p_1} &= \beta_n p_2 - 4\alpha_n p_1 \\
\dot{p_2} &= 4\alpha_n p_1 + 2\beta_n p_3 - (\beta_n + 3\alpha_n) p_2 \\
\dot{p_3} &= 3\alpha_n p_2 + 3\beta_n p_4 - (2\beta_n + 2\alpha_n) p_3 \\
\dot{p_4} &= 2\alpha_n p_3 + 4\beta_n p_5 - (3\beta_n + \alpha_n) p_4 \\
\dot{p_5} &= \alpha_n p_4 - 4\beta_n p_5 \,.
\end{aligned} \tag{5.26}$$

A solution for these equations can be constructed if we recall that, in the

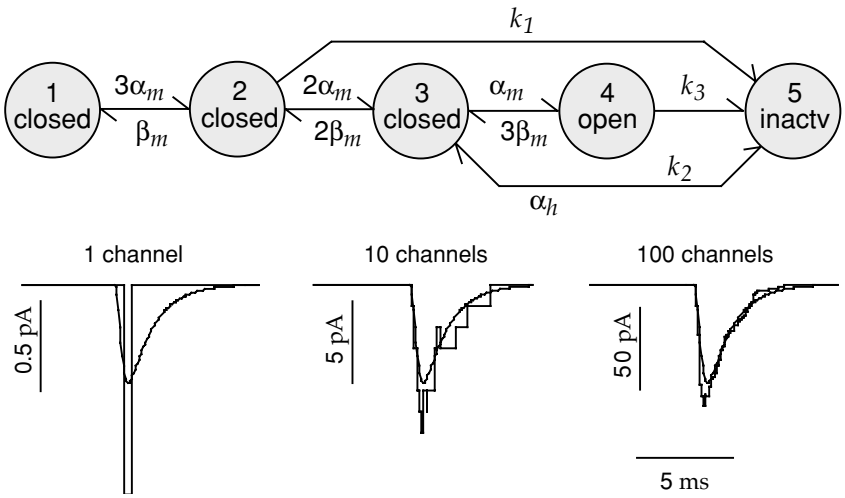

Figure 5.13 A model of the fast Na^+ channel. The upper diagram shows the states and transitions rates of the model. The values $k_1 = 0.24/\text{ms}$, $k_2 = 0.4/\text{ms}$, and $k_3 = 1.5/\text{ms}$ were used in the simulations shown in the lower panels. For these simulations, the membrane potential was initially held at -100 mV, then held at 10 mV for 20 ms, and finally returned to a holding potential of -100 mV. The smooth curves in these panels show the current predicted by the Hodgkin-Huxley model in this situation. The left panel shows a simulation of a single channel that opened once during the depolarization. The middle panel shows the total current from 10 simulated channels, and the right panel corresponds to 100 channels. As the number of channels increases, the Hodgkin-Huxley model provides a fairly accurate description of the current, but it is not identical to the channel model in this case.

Hodgkin-Huxley model, n is the probability of a subunit gate being in the open state and $1 - n$ is the probability of it being closed. If we use that same notation here, state 1 has four closed subunit gates, and thus $p_1 = (1 - n)^4$. State 5, the open state, has four open subunit gates, so $p_5 = n^4 = P$. State 2 has one open subunit gate, which can be any one of the four subunit gates, and three closed states, making $p_2 = 4n(1 - n)^3$. Similar arguments yield $p_3 = 6n^2(1 - n)^2$ and $p_4 = 4n^3(1 - n)$. These expressions generate a solution to the above equations, provided that n satisfies equation 5.16, as the reader can verify.

In the Hodgkin-Huxley model of the Na^+ conductance, the activation and inactivation processes are assumed to act independently. The schematic in figure 5.8B, which cartoons the mechanism believed to be responsible for inactivation, suggests that this assumption is incorrect. The ball that inactivates the channel is located inside the cell membrane, where it cannot be affected directly by the potential across the membrane. Furthermore, in this scheme the ball cannot occupy the channel pore until the activation gate has opened, making the two processes interdependent.

state-dependent inactivation

The state diagram in figure 5.13 reflects this by having a state-dependent, voltage-independent inactivation mechanism. This diagram is a simplified version of an Na^+ channel model due to Patlak (1991). The sequence of transitions that lead to channel opening through states 1, 2, 3, and 4 is

identical to that of the Hodgkin-Huxley model, with transition rates determined by the Hodgkin-Huxley functions $\alpha_m(V)$ and $\beta_m(V)$ and appropriate combinatoric factors. State 4 is the open state. The transition to the inactivated state 5, however, is quite different from the inactivation process in the Hodgkin-Huxley model. Inactivation transitions to state 5 can occur only from states 2, 3, and 4, and the corresponding transition rates k_1, k_2, and k_3 are constants, independent of voltage. The deinactivation process occurs at the Hodgkin-Huxley rate $\alpha_h(V)$ from state 5 to state 3.

Figure 5.13 shows simulations of this Na^+ channel model. In contrast to the K^+ channel model shown in figure 5.12, this model does not reproduce exactly the results of the Hodgkin-Huxley model when large numbers of channels are summed. Nevertheless, the two models agree quite well, as seen in the lower right panel of figure 5.13. The agreement, despite the different mechanisms of inactivation, is due to the speed of the activation process for the Na^+ conductance. The inactivation rate function $\beta_h(V)$ in the Hodgkin-Huxley model has a sigmoidal form similar to the asymptotic activation function $m_\infty(V)$ (see equation 5.24). This is indicative of the actual dependence of inactivation on m and not on V. However, the activation variable m of the Hodgkin-Huxley model reaches its voltage-dependent asymptotic value $m_\infty(V)$ so rapidly that it is difficult to distinguish inactivation processes that depend on m from those that depend on V. Differences between the two models are apparent only during a submillisecond time period while the conductance is activating. Experiments that can resolve this time scale support the channel model over the original Hodgkin-Huxley description.

5.8 Synaptic Conductances

Synaptic transmission at a spike-mediated chemical synapse begins when an action potential invades the presynaptic terminal and activates voltage-dependent Ca^{2+} channels, leading to a rise in the concentration of Ca^{2+} within the terminal. This causes vesicles containing transmitter molecules to fuse with the cell membrane and release their contents into the synaptic cleft between the pre- and postsynaptic sides of the synapse. The transmitter molecules then diffuse across the cleft and bind to receptors on the postsynaptic neuron. Binding of transmitter molecules leads to the opening of ion channels that modify the conductance of the postsynaptic neuron, completing the transmission of the signal from one neuron to the other. Postsynaptic ion channels can be activated directly by binding to the transmitter, or indirectly when the transmitter binds to a distinct receptor that affects ion channels through an intracellular second-messenger signaling pathway.

As with a voltage-dependent conductance, a synaptic conductance can be written as the product of a maximal conductance and an open channel probability, $g_s = \overline{g}_s P$. The open probability for a synaptic conductance can be expressed as a product of two terms that reflect processes occurring on

the pre- and postsynaptic sides of the synapse, $P = P_s P_{rel}$. The factor P_s is the probability that a postsynaptic channel opens, given that the transmitter was released by the presynaptic terminal. Because there are typically many postsynaptic channels, this can also be taken as the fraction of channels opened by the transmitter.

synaptic open probability P_s

P_{rel} is related to the probability that transmitter is released by the presynaptic terminal following the arrival of an action potential. This reflects the fact that transmitter release is a stochastic process. Release of transmitter at a presynaptic terminal does not necessarily occur every time an action potential arrives and, conversely, spontaneous release can occur even in the absence of the depolarization due to an action potential. The interpretation of P_{rel} is a bit subtle because a synaptic connection between neurons may involve multiple anatomical synapses, and each of these may have multiple independent transmitter release sites. The factor P_{rel}, in our discussion, is the average of the release probabilities at each release site. If there are many release sites, the total amount of transmitter released by all the sites is proportional to P_{rel}. If there is a single release site, P_{rel} is the probability that it releases transmitter. We will restrict our discussion to these two interpretations of P_{rel}. For a modest number of release sites with widely varying release probabilities, the current we discuss describes only an average over multiple trials.

transmitter release probability P_{rel}

Synapses can exert their effects on the soma, dendrites, axon spike-initiation zone, or presynaptic terminals of their postsynaptic targets. There are two broad classes of synaptic conductances that are distinguished by whether the transmitter binds to the synaptic channel and activates it directly, or the transmitter binds to a distinct receptor that activates the conductance indirectly through an intracellular signaling pathway. The first class is called ionotropic and the second, metabotropic. Ionotropic conductances activate and deactivate more rapidly than metabotropic conductances. Metabotropic receptors can, in addition to opening channels, cause long-lasting changes inside a neuron. They typically operate through pathways that involve G-protein-mediated receptors and various intracellular signaling molecules known as second messengers. Many neuromodulators, including serotonin, dopamine, norepinephrine, and acetylcholine, act through metabotropic receptors. These have a wide variety of important effects on the functioning of the nervous system.

ionotropic receptor

metabotropic receptor

Glutamate and GABA (γ-aminobutyric acid) are the major excitatory and inhibitory transmitters in the brain. Both act ionotropically and metabotropically. The principal ionotropic receptor types for glutamate are called AMPA and NMDA. Both AMPA and NMDA receptors produce mixed-cation conductances with reversal potentials around 0 mV. The AMPA current activates and deactivates rapidly. The NMDA receptor is somewhat slower to activate and deactivates considerably more slowly. In addition, NMDA receptors have an unusual voltage dependence that we discuss in a later section, and are more permeable to Ca^{2+} than AMPA receptors.

glutamate, GABA

AMPA, NMDA

GABA$_A$, *GABA*$_B$

GABA activates two important inhibitory synaptic conductances in the brain. $GABA_A$ receptors produce a relatively fast ionotropic Cl^- conductance. $GABA_B$ receptors are metabotropic, and act to produce a slower and longer-lasting K^+ conductance.

gap junctions

In addition to chemical synapses, neurons can be coupled through electrical synapses (gap junctions) that produce a synaptic current proportional to the difference between the pre- and postsynaptic membrane potentials. Some gap junctions rectify so that positive and negative current flows are not equal for potential differences of the same magnitude.

The Postsynaptic Conductance

In a simple model of a directly activated receptor channel, the transmitter interacts with the channel through a binding reaction in which k transmitter molecules bind to a closed receptor and open it. In the reverse reaction, the transmitter molecules unbind from the receptor and it closes. These processes are analogous to the opening and closing involved in the gating of a voltage-dependent channel, and the same type of equation is used to describe how the open probability P_s changes with time,

$$\frac{dP_s}{dt} = \alpha_s(1 - P_s) - \beta_s P_s \,. \tag{5.27}$$

Here, β_s determines the closing rate of the channel and is usually assumed to be a constant. The opening rate, α_s, on the other hand, depends on the concentration of transmitter available for binding to the receptor. If the concentration of transmitter at the site of the synaptic channel is [transmitter], the probability of finding k transmitter molecules within binding range of the channel is proportional to [transmitter]^k, and α_s is some constant of proportionality times this factor.

When an action potential invades the presynaptic terminal, the transmitter concentration rises and α_s grows rapidly, causing P_s to increase. Following the release of transmitter, diffusion out of the cleft, enzyme-mediated degradation, and presynaptic uptake mechanisms can all contribute to a rapid reduction of the transmitter concentration. This sets α_s to 0, and P_s follows suit by decaying exponentially with a time constant $1/\beta_s$. Typically, the time constant for channel closing is considerably larger than the opening time.

As a simple model of transmitter release, we assume that the transmitter concentration in the synaptic cleft rises extremely rapidly after vesicle release, remains at a high value for a period of duration T, and then falls rapidly to 0. Thus, the transmitter concentration is modeled as a square pulse. While the transmitter concentration is nonzero, α_s takes a constant value much greater than β_s, otherwise $\alpha_s = 0$. Suppose that vesicle release occurs at time $t = 0$ and that the synaptic channel open probability takes the value $P_s(0)$ at this time. While the transmitter concentration in the cleft

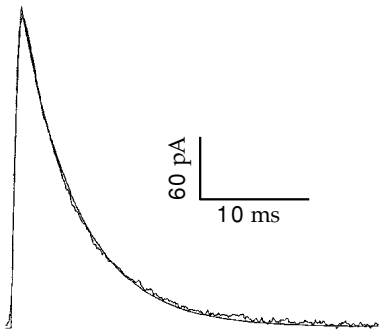

Figure 5.14 A fit of the model discussed in the text to the average EPSC (excitatory postsynaptic current) recorded from mossy fiber input to a CA3 pyramidal cell in a hippocampal slice preparation. The smooth line is the theoretical curve and the wiggly line is the result of averaging recordings from a number of trials. (Adapted from Destexhe et al., 1994.)

is nonzero, α_s is so much larger than β_s that we can ignore the term involving β_s in equation 5.27. Integrating equation 5.27 under this assumption, we find that

$$P_s(t) = 1 + (P_s(0) - 1)\exp(-\alpha_s t) \quad \text{for} \quad 0 \le t \le T\,. \tag{5.28}$$

The open probability takes its maximum value at time $t = T$ and then, for $t \ge T$, decays exponentially at a rate determined by the constant β_s,

$$P_s(t) = P_s(T)\exp(-\beta_s(t - T)) \quad \text{for} \quad t \ge T\,. \tag{5.29}$$

If $P_s(0) = 0$, as it will if there is no synaptic release immediately before the release at $t = 0$, equation 5.28 simplifies to $P_s(t) = 1 - \exp(-\alpha_s t)$ for $0 \le t \le T$, and this reaches a maximum value $P_{\max} = P_s(T) = 1 - \exp(-\alpha_s T)$. In terms of this parameter, a simple manipulation of equation 5.28 shows that we can write, in the general case,

$$P_s(T) = P_s(0) + P_{\max}(1 - P_s(0))\,. \tag{5.30}$$

Figure 5.14 shows a fit to a recorded postsynaptic current using this formalism. In this case, β_s was set to 0.19 ms^{-1}. The transmitter concentration was modeled as a square pulse of duration $T = 1$ ms during which $\alpha_s = 0.93$ ms^{-1}. Inverting these values, we find that the time constant determining the rapid rise seen in figure 5.14A is 0.9 ms, while the fall of the current is an exponential with a time constant of 5.26 ms.

For a fast synapse like the one shown in figure 5.14, the rise of the conductance following a presynaptic action potential is so rapid that it can be approximated as instantaneous. In this case, the synaptic conductance due to a single presynaptic action potential occurring at $t = 0$ is often written as an exponential, $P_s = P_{\max}\exp(-t/\tau_s)$ (see the AMPA trace in figure 5.15A), where from equation 5.29, $\tau_s = 1/\beta_s$. The synaptic conductance due to a

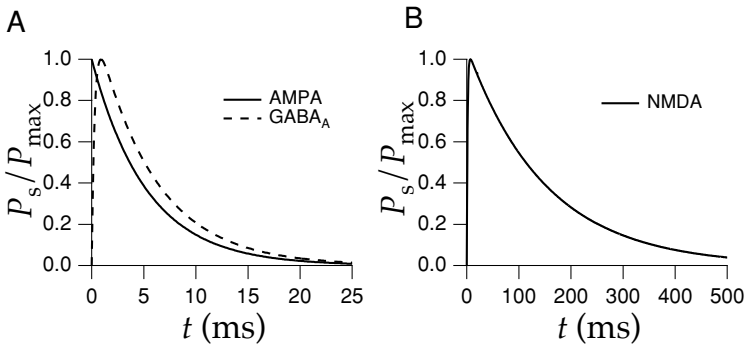

Figure 5.15 Time-dependent open probabilities fitted to match AMPA, $GABA_A$, and NMDA synaptic conductances. (A) The AMPA curve is a single exponential described by equation 5.31 with $\tau_s = 5.26$ ms. The $GABA_A$ curve is a difference of exponentials with $\tau_1 = 5.6$ ms and $\tau_{rise} = 0.3$ ms. (B) The NMDA curve is the differences of two exponentials with $\tau_1 = 152$ ms and $\tau_{rise} = 1.5$ ms. (Parameters are from Destexhe et al., 1994.)

sequence of action potentials at arbitrary times can be modeled by allowing P_s to decay exponentially to 0 according to the equation

$$\tau_s \frac{dP_s}{dt} = -P_s \,, \tag{5.31}$$

and, on the basis of the equation 5.30, making the replacement

$$P_s \rightarrow P_s + P_{max}(1 - P_s) \tag{5.32}$$

immediately after each presynaptic action potential.

Equations 5.28 and 5.29 can also be used to model synapses with slower rise times, but other functional forms are often used. One way of describing both the rise and the fall of a synaptic conductance is to express P_s as the difference of two exponentials (see the $GABA_A$ and NMDA traces in figure 5.15). For an isolated presynaptic action potential occurring at $t = 0$, the synaptic conductance is written as

$$P_s = P_{max} B \left(\exp(-t/\tau_1) - \exp(-t/\tau_2) \right) \,, \tag{5.33}$$

where $\tau_1 > \tau_2$, and B is a normalization factor that assures that the peak value of P_s is equal to P_{max},

$$B = \left(\left(\frac{\tau_2}{\tau_1} \right)^{\tau_{rise}/\tau_1} - \left(\frac{\tau_2}{\tau_1} \right)^{\tau_{rise}/\tau_2} \right)^{-1} . \tag{5.34}$$

The rise time of the synapse is determined by $\tau_{rise} = \tau_1 \tau_2 / (\tau_1 - \tau_2)$, while the fall time is set by τ_1. This conductance reaches its peak value $\tau_{rise} \ln(\tau_1/\tau_2)$ after the presynaptic action potential.

Another way of describing a synaptic conductance is to use the expression

$$P_s = \frac{P_{max} t}{\tau_s} \exp(1 - t/\tau_s) \tag{5.35}$$

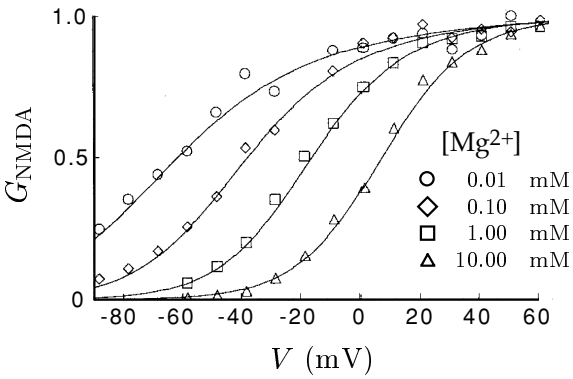

Figure 5.16 Dependence of the NMDA conductance on the membrane potential and extracellular Mg^{2+} concentration. Normal extracellular Mg^{2+} concentrations are in the range of 1 to 2 mM. The solid lines are the factors G_{NMDA} of equation 5.36 for different values of $[Mg^{2+}]$, and the symbols indicate the data points. (Adapted from Jahr and Stevens, 1990.)

for an isolated presynaptic release that occurs at time $t = 0$. This expression, called an alpha function, starts at 0, reaches its peak value at $t = \tau_s$, and then decays with a time constant τ_s. *alpha function*

We mentioned earlier in this chapter that NMDA receptor conductance has an additional dependence on the postsynaptic potential not normally seen in other conductances. To incorporate this dependence, the current due to the NMDA receptor can be described using an additional factor that depends on the postsynaptic potential, V. The NMDA current is written as $\overline{g}_{\mathrm{NMDA}} G_{\mathrm{NMDA}}(V) P (V - E_{\mathrm{NMDA}})$. P is the usual open probability factor. The factor $G_{\mathrm{NMDA}}(V)$ describes an extra voltage dependence due to the fact that when the postsynaptic neuron is near its resting potential, NMDA receptors are blocked by Mg^{2+} ions. To activate the conductance, the postsynaptic neuron must be depolarized to knock out the blocking ions. Jahr and Stevens (1990) have fitted this dependence by (figure 5.16) *NMDA receptor*

$$G_{\mathrm{NMDA}} = \left(1 + \frac{[\mathrm{Mg}^{2+}]}{3.57\ \mathrm{mM}} \exp(-V/16.13\ \mathrm{mV})\right)^{-1}. \qquad (5.36)$$

NMDA receptors conduct Ca^{2+} ions as well as monovalent cations. Entry of Ca^{2+} ions through NMDA receptors is a critical event for long-term modification of synaptic strength. The fact that the opening of NMDA channels requires both pre- and postsynaptic depolarization means NMDA receptors can act as coincidence detectors of simultaneous pre- and postsynaptic activity. This plays an important role in connection with the Hebb rule for synaptic modification discussed in chapter 8. *coincidence detection*

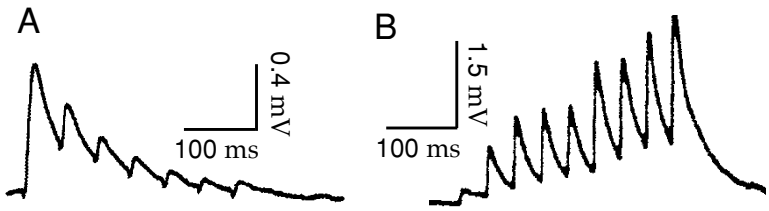

Figure 5.17 Depression and facilitation of excitatory intracortical synapses. (A) Depression of an excitatory synapse between two layer 5 pyramidal cells recorded in a slice of rat somatosensory cortex. Spikes were evoked by current injection into the presynaptic neuron, and postsynaptic potentials were recorded with a second electrode. (B) Facilitation of an excitatory synapse from a pyramidal neuron to an inhibitory interneuron in layer 2/3 of rat somatosensory cortex. (A from Markram and Tsodyks, 1996; B from Markram et al., 1998.)

Release Probability and Short-Term Plasticity

short-term plasticity

long-term plasticity

The probability of transmitter release and the magnitude of the resulting conductance change in the postsynaptic neuron can depend on the history of activity at a synapse. The effects of activity on synaptic conductances are termed short- and long-term. Short-term plasticity refers to a number of phenomena that affect the probability that a presynaptic action potential opens postsynaptic channels and that last anywhere from milliseconds to tens of seconds. The effects of long-term plasticity are extremely persistent, lasting, for example, as long as the preparation being studied can be kept alive. The modeling and implications of long-term plasticity are considered in chapter 8. Here we present a simple way of describing short-term synaptic plasticity as a modification in the release probability for synaptic transmission. Short-term modifications of synaptic transmission can involve other mechanisms than merely changes in the probability of transmission, but for simplicity we absorb all these effects into a modification of the factor P_{rel} introduced previously. Thus, P_{rel} can be interpreted more generally as a presynaptic factor affecting synaptic transmission.

depression facilitation

Figure 5.17 illustrates two principal types of short-term plasticity, depression and facilitation. Figure 5.17A shows trial-averaged postsynaptic current pulses produced in one cortical pyramidal neuron by evoking a regular series of action potentials in a second pyramidal neuron presynaptic to the first. The pulses dramatically decrease in amplitude upon repeated activation of the synaptic conductance, revealing short-term synaptic depression. Figure 5.17B shows a similar series of averaged postsynaptic current pulses recorded in a cortical inhibitory interneuron when a sequence of action potentials was evoked in a presynaptic pyramidal cell. In this case, the amplitude of the pulses increases, and thus the synapse facilitates. In general, synapses can exhibit facilitation and depression over a variety of time scales, and multiple components of short-term plasticity can be found at the same synapse. To keep the discussion simple, we consider synapses that exhibit either facilitation or depression described by a single time constant.

Facilitation and depression can both be modeled as presynaptic processes that modify the probability of transmitter release. We describe them using a simple nonmechanistic model that has similarities to the model of P_s presented in the previous subsection. For both facilitation and depression, the release probability after a long period of presynaptic silence is $P_{\rm rel} = P_0$. Activity at the synapse causes $P_{\rm rel}$ to increase in the case of facilitation and to decrease for depression. Between presynaptic action potentials, the release probability decays exponentially back to its "resting" value, P_0,

$$\tau_{\rm P}\frac{dP_{\rm rel}}{dt} = P_0 - P_{\rm rel}\,. \tag{5.37}$$

The parameter $\tau_{\rm P}$ controls the rate at which the release probability decays to P_0.

The models of facilitation and depression differ in how the release probability is changed by presynaptic activity. In the case of facilitation, $P_{\rm rel}$ is augmented by making the replacement $P_{\rm rel} \to P_{\rm rel} + f_{\rm F}(1 - P_{\rm rel})$ immediately after a presynaptic action potential (as in equation 5.32). The parameter $f_{\rm F}$ (with $0 \le f_{\rm F} \le 1$) controls the degree of facilitation, and the factor $(1 - P_{\rm rel})$ prevents the release probability from growing larger than 1. To model depression, the release probability is reduced after a presynaptic action potential by making the replacement $P_{\rm rel} \to f_{\rm D}P_{\rm rel}$. In this case, the parameter $f_{\rm D}$ (with $0 \le f_{\rm D} \le 1$) controls the amount of depression, and the factor $P_{\rm rel}$ prevents the release probability from becoming negative.

We begin by analyzing the effects of facilitation on synaptic transmission for a presynaptic spike train with Poisson statistics. In particular, we compute the average steady-state release probability, denoted by $\langle P_{\rm rel}\rangle$. $\langle P_{\rm rel}\rangle$ is determined by requiring that the facilitation that occurs after each presynaptic action potential is exactly canceled by the average exponential decrement that occurs between presynaptic spikes. Consider two presynaptic action potentials separated by an interval τ, and suppose that the release probability takes its average value value $\langle P_{\rm rel}\rangle$ at the time of the first spike. Immediately after this spike, it is augmented to $\langle P_{\rm rel}\rangle + f_{\rm F}(1 - \langle P_{\rm rel}\rangle)$. By the time of the second spike, this will have decayed to $P_0 + (\langle P_{\rm rel}\rangle + f_{\rm F}(1 - \langle P_{\rm rel}\rangle) - P_0)\exp(-\tau/\tau_{\rm P})$, which is obtained by integrating equation 5.37. The average value of the exponential decay factor in this expression is the integral over all positive τ values of $\exp(-\tau/\tau_{\rm P})$ times the probability density for a Poisson spike train with a firing rate r to produce an interspike interval of duration τ, which is $r\exp(-r\tau)$ (see chapter 1). Thus, the average exponential decrement is

$$r\int_0^\infty d\tau\ \exp(-r\tau - \tau/\tau_{\rm P}) = \frac{r\tau_{\rm P}}{1 + r\tau_{\rm P}}\,. \tag{5.38}$$

In order for the release probability to return, on average, to its steady-state value between presynaptic spikes, we must therefore require that

$$\langle P_{\rm rel}\rangle = P_0 + \left(\langle P_{\rm rel}\rangle + f_{\rm F}(1 - \langle P_{\rm rel}\rangle) - P_0\right)\frac{r\tau_{\rm P}}{1 + r\tau_{\rm P}}\,. \tag{5.39}$$

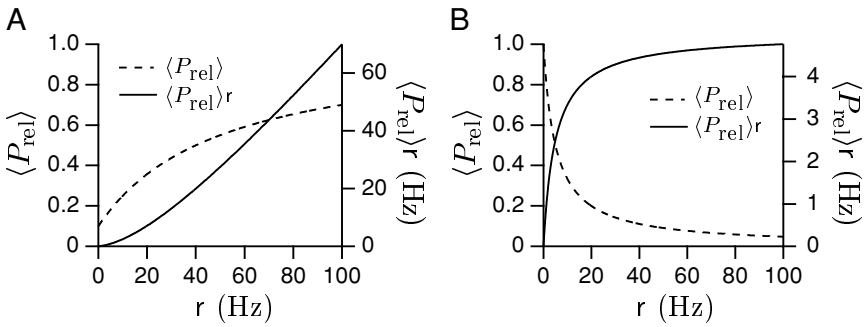

Figure 5.18 The effects of facilitation and depression on synaptic transmission. (A) Release probability and transmission rate for a facilitating synapse as a function of the firing rate of a Poisson presynaptic spike train. The dashed curve shows the rise of the average release probability as the presynaptic rate increases. The solid curve is the average rate of transmission, which is the average release probability times the presynaptic firing rate. The parameters of the model are $P_0 = 0.1$, $f_{\rm F} = 0.4$, and $\tau_{\rm P} = 50$ ms. (B) Same as A, but for the case of depression. The parameters of the model are $P_0 = 1$, $f_{\rm D} = 0.4$, and $\tau_{\rm P} = 500$ ms.

Solving for $\langle P_{\rm rel}\rangle$ gives

$$\langle P_{\rm rel}\rangle = \frac{P_0 + f_{\rm F} {\rm r} \tau_{\rm P}}{1 + {\rm r} f_{\rm F} \tau_{\rm P}} \,. \tag{5.40}$$

This equals P_0 at low rates and rises toward the value 1 at high rates (figure 5.18A). As a result, isolated spikes in low-frequency trains are transmitted with lower probability than spikes occurring within high-frequency bursts. The synaptic transmission rate when the presynaptic neuron is firing at rate r is the firing rate times the release probability. This is approximately P_0r for small rates and approaches r at high rates (figure 5.18A).

The value of $\langle P_{\rm rel}\rangle$ for a Poisson presynaptic spike train can also be computed in the case of depression. The only difference from the above derivation is that following a presynaptic spike, $\langle P_{\rm rel}\rangle$ is decreased to $f_{\rm D}\langle P_{\rm rel}\rangle$. Thus, the consistency condition 5.39 is replaced by

$$\langle P_{\rm rel}\rangle = P_0 + (f_{\rm D}\langle P_{\rm rel}\rangle - P_0)\frac{{\rm r}\tau_{\rm P}}{1 + {\rm r}\tau_{\rm P}} \,, \tag{5.41}$$

giving

$$\langle P_{\rm rel}\rangle = \frac{P_0}{1 + (1 - f_{\rm D}){\rm r}\tau_{\rm P}} \,. \tag{5.42}$$

This equals P_0 at low rates and decreases as $1/{\rm r}$ at high rates (figure 5.18B), which has some interesting consequences. As noted above, the average rate of successful synaptic transmissions is equal to $\langle P_{\rm rel}\rangle$ times the presynaptic rate r. Because $\langle P_{\rm rel}\rangle$ is proportional to $1/{\rm r}$ at high rates, the average transmission rate is independent of r in this range. This can be seen by the flattening of the solid curve in figure 5.18B. As a result, synapses

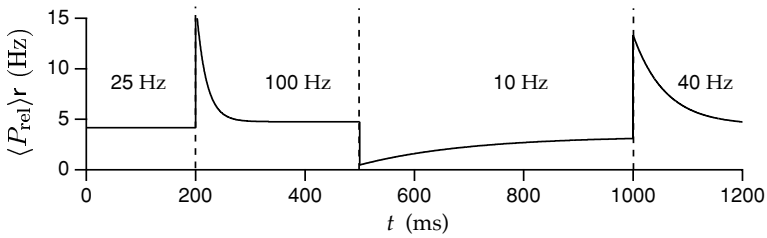

Figure 5.19 The average rate of transmission for a synapse with depression when the presynaptic firing rate changes in a sequence of steps. The firing rates were held constant at the values 25, 100, 10, and 40 Hz, except for abrupt changes at the times indicated by the dashed lines. The parameters of the model are $P_0 = 1$, $f_D = 0.6$, and $\tau_P = 500$ ms.

that depress do not convey information about the values of constant, high presynaptic firing rates to their postsynaptic targets. The presynaptic firing rate at which transmission starts to become independent of r is around $1/((1 - f_D)\tau_P)$.

Figure 5.19 shows the average transmission rate, $\langle P_{\rm rel}\rangle$r, in response to a series of steps in the presynaptic firing rate. Note first that the steady-state transmission rates during the 25, 100, 10, and 40 Hz periods are quite similar. This is a consequence of the $1/$r dependence of the average release probability, as discussed above. The largest transmission rates in the figure occur during the sharp upward transitions between different presynaptic rates. This illustrates the important point that depressing synapses amplify transient signals relative to steady-state inputs. The transients corresponding the 25 to 100 Hz transition and the 10 to 40 Hz transition are of roughly equal amplitudes, but the transient for the 10 to 40 Hz transition is broader than that for the 25 to 100 Hz transition.

The equality of amplitudes of the two upward transients in figure 5.19 is a consequence of the $1/$r behavior of $\langle P_{\rm rel}\rangle$. Suppose that the presynaptic firing rate makes a sudden transition from a steady value r to a new value $\mathsf{r} + \Delta\mathsf{r}$. Before the transition, the average release probability is given by equation 5.42. Immediately after the transition, before the release probability has had time to adjust to the new input rate, the average transmission rate will be this previous value of $\langle P_{\rm rel}\rangle$ times the new rate $\mathsf{r} + \Delta\mathsf{r}$, which is $P_0(r + \Delta r)/(1 + (1 - f_D)r\tau_P)$. For sufficiently high rates, this is approximately proportional to $(\mathsf{r} + \Delta\mathsf{r})/\mathsf{r}$. The size of the change in the transmission rate is thus proportional to $\Delta\mathsf{r}/\mathsf{r}$, which means that depressing synapses not only amplify transient inputs, they transmit them in a scaled manner. The amplitude of the transient transmission rate is proportional to the fractional change, not the absolute change, in the presynaptic firing rate. The two transients seen in figure 5.19 have similar amplitudes because in both cases $\Delta r/r = 3$. The difference in the recovery time for the two upward transients in figure 5.19 is due to the fact that the effective time constant governing the recovery to a new steady-state level r is $\tau_P/(1 + (1 - f_D)\tau_P r)$.

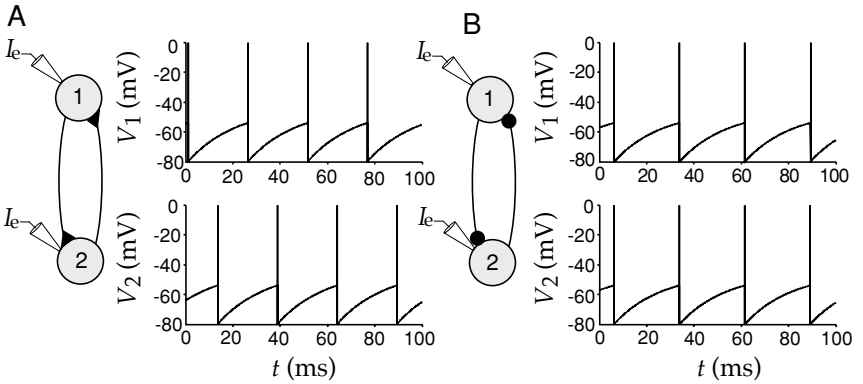

Figure 5.20 Two synaptically coupled integrate-and-fire neurons. (A) Excitatory synapses (E_s = 0 mV) produce an alternating, out-of-phase pattern of firing. (B) Inhibitory synapses (E_s = -80 mV) produce synchronous firing. Both model neurons have E_L = -70 mV, V_{th} = -54 mV, V_{reset} = -80 mV, τ_m = 20 ms, $r_m\overline{g}_s$ = 0.05, P_{max} = 1, $R_m I_e$ = 25 mV, and τ_s = 10 ms.

5.9 Synapses on Integrate-and-Fire Neurons

Synaptic inputs can be incorporated into an integrate-and-fire model by including synaptic conductances in the membrane current appearing in equation 5.8,

$$\tau_m \frac{dV}{dt} = E_L - V - r_m\overline{g}_s P_s(V - E_s) + R_m I_e \,. \tag{5.43}$$

For simplicity, we assume that $P_{rel} = 1$ in this example. The synaptic current is multiplied by r_m in equation 5.43 because equation 5.8 was multiplied by this factor. To model synaptic transmission, P_s changes whenever the presynaptic neuron fires an action potential using one of the schemes described previously.

synchronous and asynchronous firing

Figures 5.20A and 5.20B show examples of two integrate-and-fire neurons driven by electrode currents and connected by identical excitatory or inhibitory synapses. The synaptic conductances in this example are described by the α function model. This means that the synaptic conductance a time t after the occurrence of a presynaptic action potential is given by equation 5.35. The figure shows a nonintuitive effect. When the synaptic time constant is sufficiently long (τ_s = 10 ms in this example), excitatory connections produce a state in which the two neurons fire alternately, out of phase with one another, while inhibitory synapses produce synchronous firing. It is normally assumed that excitation produces synchrony. Actually, in some cases inhibitory connections can be more effective than excitatory connections at synchronizing neuronal firing.

Synapses have multiple effects on their postsynaptic targets. In equation 5.43, the term $r_m\overline{g}_s P_s E_s$ acts as a source of current to the neuron, while

the term $r_m \overline{g}_s P_s V$ changes the membrane conductance. The effects of the latter term are referred to as shunting, and they can be identified most easily if we divide equation 5.43 by $1 + r_m \overline{g}_s P_s$ to obtain

$$\frac{\tau_m}{1 + r_m \overline{g}_s P_s} \frac{dV}{dt} = -V + \frac{E_L + r_m \overline{g}_s P_s E_s + R_m I_e}{1 + r_m \overline{g}_s P_s}. \tag{5.44}$$

The shunting effects of the synapse are seen in this equation as a decrease in the effective membrane time constant, and a divisive reduction in the impact of the leakage and synaptic reversal potentials and of the electrode current.

The shunting effects seen in equation 5.44 have been proposed as a possible basis for neural computations involving division. However, shunting has a divisive effect only on the membrane potential of an integrate-and-fire neuron; its effect on the firing rate is subtractive. To see this, assume that synaptic input is arriving at a sufficient rate to maintain a relatively constant value of P_s. In this case, shunting amounts to changing the value of the membrane resistance from R_m to $R_m/(1 + r_m \overline{g}_s P_s)$. Recalling equation 5.12 for the firing rate of the integrate-and-fire model, and the fact that $\tau_m = C_m R_m$, we can write the firing rate in a form that reveals its dependence on R_m,

$$r_{isi} \approx \left[\frac{E_L - V_{th}}{C_m R_m (V_{th} - V_{reset})} + \frac{I_e}{C_m (V_{th} - V_{reset})} \right]_+ . \tag{5.45}$$

Changing R_m modifies only the constant term in this equation; it has no effect on the dependence of the firing rate on I_e.

Regular and Irregular Firing Modes

Integrate-and-fire models are useful for studying how neurons sum large numbers of synaptic inputs and how networks of neurons interact. One issue that has received considerable attention is the degree of variability in the firing output of integrate-and-fire neurons receiving synaptic input. This work has led to the realization that neurons can respond to multiple synaptic inputs in two different modes of operation depending on the balance that exists between excitatory and inhibitory contributions.

The two modes of operation are illustrated in figure 5.21, which shows membrane potentials of an integrate-and-fire model neuron responding to 1000 excitatory and 200 inhibitory inputs. Each input consists of an independent Poisson spike train driving a synaptic conductance. The upper panels of figure 5.21 show the membrane potential with the action potential generation mechanism of the model turned off, and figures 5.21A and 5.21B illustrate the two different modes of operation. In figure 5.21A, the effect of the excitatory inputs is strong enough, relative to that of the inhibitory inputs, to make the average membrane potential, when action

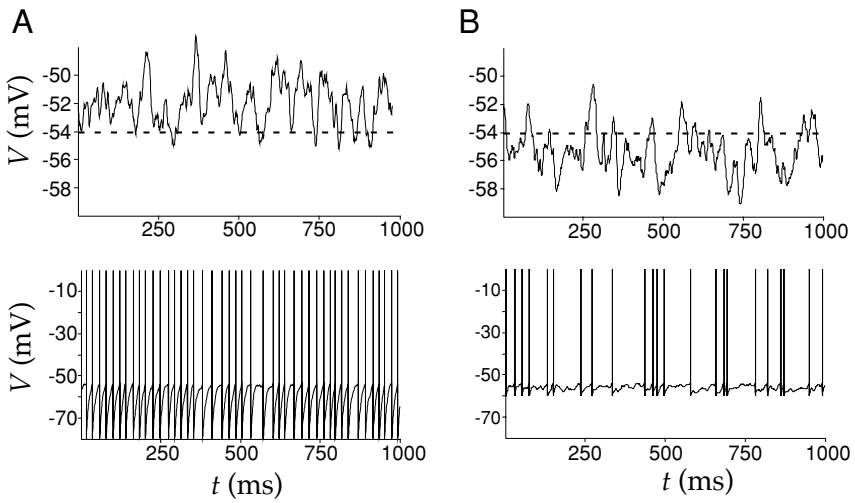

Figure 5.21 The regular and irregular firing modes of an integrate-and-fire model neuron. (A) The regular firing mode. Upper panel: The membrane potential of the model neuron when the spike generation mechanism is turned off. The average membrane potential is above the spiking threshold (dashed line). Lower panel: When the spike generation mechanism is turned on, it produces a regular spiking pattern. (B) The irregular firing mode. Upper panel: The membrane potential of the model neuron when the spike generation mechanism is turned off. The average membrane potential is below the spiking threshold (dashed line). Lower panel: When the spike generation mechanism is turned on, it produces an irregular spiking pattern. In order to keep the firing rates from differing too greatly between these two examples, the value of the reset voltage is higher in B than in A.

potential generation is blocked, more depolarized than the spiking threshold of the model (the dashed line in the figure). When the action potential mechanism is turned on (lower panel of figure 5.21A), this produces a fairly regular pattern of action potentials.

The irregularity of a spike train can be quantified using the coefficient of variation (C_V), the ratio of the standard deviation to the mean of the interspike intervals (see chapter 1). For the Poisson inputs being used in this example, $C_V = 1$, while for the spike train in the lower panel of figure 5.21A, $C_V = 0.3$. Thus, the output spike train is much more regular than the input trains. This is not surprising, because the model neuron effectively averages its many synaptic inputs. In the regular firing mode, the total synaptic input attempts to charge the neuron above the threshold, but every time the potential reaches the threshold, it gets reset and starts charging again. In this mode of operation, the timing of the action potentials is determined primarily by the charging rate of the cell, which is controlled by its membrane time constant.

Figure 5.21B shows the other mode of operation that produces an irregular firing pattern. In the irregular firing mode, the average membrane potential is more hyperpolarized than the threshold for action potential generation (upper panel of figure 5.21B). Action potentials are generated

only when there is a fluctuation in the total synaptic input strong enough to make the membrane potential reach the threshold. This produces an irregular spike train, such as that seen in the lower panel of figure 5.21B, which has a C_V value of 0.84.

The high degree of variability seen in the spiking patterns of in vivo recordings of cortical neurons (see chapter 1) suggests that they are better approximated by an integrate-and-fire model operating in an irregular-firing mode. There are advantages to operating in the irregular-firing mode that may compensate for its increased variability. One is that neurons firing in the irregular mode reflect in their outputs the temporal properties of fluctuations in their total synaptic input. In the regular firing mode, the timing of output spikes is only weakly related to the temporal character of the input spike trains. In addition, neurons operating in the irregular firing mode can respond more quickly to changes in presynaptic spiking patterns and firing rates than those operating in the regular firing mode.

5.10 Chapter Summary

In this chapter, we considered the basic electrical properties of neurons, including their intracellular and membrane resistances, capacitances, and active voltage-dependent and synaptic conductances. We introduced the Nernst equation for equilibrium potentials and the formalism of Hodgkin and Huxley for describing persistent, transient, and hyperpolarization-activated conductances. Methods were introduced for modeling stochastic channel opening and stochastic synaptic transmission, including the effects of synaptic facilitation and depression. We discussed a number of ways of describing synaptic conductances following the release of a neurotransmitter. Two models of action potential generation were discussed, the simple integrate-and-fire scheme and the more realistic Hodgkin-Huxley model.

5.11 Appendices

A: Integrating the Membrane Potential

We begin by considering the numerical integration of equation 5.8. It is convenient to rewrite this equation in the form

$$\tau_V \frac{dV}{dt} = V_\infty - V\,, \tag{5.46}$$

where $\tau_V = \tau_m$ and $V_\infty = E_\mathrm{L} + R_\mathrm{m} I_\mathrm{e}$. When the electrode current I_e is independent of time, the solution of this equation is

$$V(t) = V_\infty + (V(t_0) - V_\infty)\exp(-(t - t_0)/\tau_V)\,, \tag{5.47}$$

where t_0 is any time prior to t and $V(t_0)$ is the value of V at time t_0. Equation 5.9 is a special case of this result with $t_0 = 0$.

If I_e depends on time, the solution 5.47 is not valid. An analytic solution can still be written down in this case, but it is not particularly useful except in special cases. Over a small enough time period Δt, we can approximate $I_e(t)$ as constant and use the solution 5.47 to step from a time t to $t + \Delta t$. This requires replacing the variable t_0 in equation 5.47 with t, and t with $t + \Delta t$, so that

$$V(t + \Delta t) = V_\infty + (V(t) - V_\infty) \exp(-\Delta t/\tau_V) . \tag{5.48}$$

This equation provides an updating rule for the numerical integration of equation 5.46. Provided that Δt is sufficiently small, repeated application of the update rule 5.48 provides an accurate way of determining the membrane potential. Furthermore, this method is stable because if Δt is too large, it will only move V toward V_∞ and not, for example, make it grow without bound.

The equation for a general single-compartment conductance-based model, equation 5.6 with 5.5, can be written in the same form as equation 5.46 with

$$V_\infty = \frac{\sum_i g_i E_i + I_e/A}{\sum_i g_i} \tag{5.49}$$

and

$$\tau_V = \frac{c_m}{\sum_i g_i} . \tag{5.50}$$

Note that if c_m is in units of nF/mm^2 and the conductances are in the units μS/mm^2, τ_V comes out in ms units. Similarly, if the reversal potentials are given in units of mV, I_e is in nA, and A is in mm^2, V_∞ will be in mV units.

If we take the time interval Δt to be small enough so that the gating variables can be approximated as constant during this period, the membrane potential can again be integrated over one time step, using equation 5.48. Of course, the gating variables are not fixed, so once V has been updated by this rule, the gating variables must be updated as well.

B: Integrating the Gating Variables

All the gating variables in a conductance-based model satisfy equations of the same form,

$$\tau_z \frac{dz}{dt} = z_\infty - z , \tag{5.51}$$

where we use z to denote a generic variable. Note that this equation has the same form as equation 5.46, and it can be integrated in exactly the same way. We assume that Δt is sufficiently small so that V does not change appreciably over this time interval (and similarly $[Ca^{2+}]$ is approximated as

constant over this interval if any of the conductances are Ca^{2+}-dependent). Then, τ_z and z_∞, which are functions of V (and possibly $[Ca^{2+}]$) can be treated as constants over this period and z can be updated by a rule identical to 5.48,

$$z(t + \Delta t) = z_\infty + (z(t) - z_\infty) \exp(-\Delta t/\tau_z). \tag{5.52}$$

An efficient integration scheme for conductance-based models is to alternate using rule (5.48) to update the membrane potential and rule (5.52) to update all the gating variables. It is important to alternate the updating of V with that of the gating variables, rather than doing them all simultaneously, as this keeps the method accurate to second order in Δt. If Ca^{2+}-dependent conductances are included, the intracellular Ca^{2+} concentration should be computed simultaneously with the membrane potential. By alternating the updating, we mean that the membrane potential is computed at times $0, \Delta t, 2\Delta t, \ldots$, while the gating variables are computed at times $\Delta t/2, 3\Delta t/2, 5\Delta t/2, \ldots$. A discussion of the second-order accuracy of this scheme is given in Mascagni and Sherman (1998).

5.12 Annotated Bibliography

Jack et al. (1975), **Tuckwell (1988)**, **Johnston & Wu (1995)**, **Koch & Segev (1998)**, and **Koch (1998)** cover much of the material in this chapter and in chapter 6. **Hille (1992)** provides a comprehensive treatment of ion channels. **Hodgkin & Huxley (1952)** presents the classic biophysical model of the action potential, and **Sakmann & Neher (1983)** describes patch clamp recording techniques allowing single channels to be studied electrophysiologically.

The integrate-and-fire model was introduced by Lapicque (1907). **Destexhe et al. (1994)** describes kinetic models of both ion channels and short-term postsynaptic effects at synapses. Marom & Abbott (1994) shows how the Na^+ channel model of Patlak (1991) can be reconciled with typical macroscopic conductance models. For a review of the spike-response model, the integrated version of the integrate-and-fire model, see **Gerstner (1998)**. Wang (1994) analyzes a spike-rate adaptation model similar to the one we presented, and Stevens & Zador (1998) introduces an integrate-and-fire model with time-dependent parameters.

The dynamic aspects of synaptic transmission are reviewed in **Magleby (1987)** and **Zucker (1989)**. Our presentation followed Abbott et al. (1997), Varela et al. (1997), and Tsodyks & Markram (1997). For additional implications of short-term synaptic plasticity for cortical processing, see Lisman (1997) and Chance et al. (1998). Wang & Rinzel (1992) notes that inhibitory synapses can synchronize coupled cells, and in our discussion we followed the treatment in van Vreeswijk et al. (1994). Our analysis of the regular and irregular firing mode regimes of integrate-and-fire cells was

based on Troyer & Miller (1997). Numerical methods for integrating the equations of neuron models are discussed in **Mascagni & Sherman (1998)**.

6 Model Neurons II: Conductances and Morphology

6.1 Levels of Neuron Modeling

In modeling neurons, we must deal with two types of complexity: the intricate interplay of active conductances that makes neuronal dynamics so rich and interesting, and the elaborate morphology that allows neurons to receive and integrate inputs from so many other neurons. The first part of this chapter extends the material presented in chapter 5 by examining single-compartment models with a wider variety of voltage-dependent conductances, and hence a wider range of dynamic behaviors, than the Hodgkin-Huxley model. In the second part of the chapter, we introduce methods used to study the effects of morphology on the electrical characteristics of neurons. An analytic approach known as cable theory is presented first, followed by a discussion of multi-compartment models that permit numerical simulation of complex neuronal structures.

Model neurons range from greatly simplified caricatures to highly detailed descriptions involving thousands of differential equations. Choosing the most appropriate level of modeling for a given research problem requires a careful assessment of the experimental information available and a clear understanding of the research goals. Oversimplified models can, of course, give misleading results, but excessively detailed models can obscure interesting results beneath inessential and unconstrained complexity.

6.2 Conductance-Based Models

The electrical properties of neurons arise from membrane conductances with a wide variety of properties. The basic formalism developed by Hodgkin and Huxley to describe the Na^+ and K^+ conductances responsible for generating action potentials (discussed in chapter 5) is also used to represent most of the additional conductances encountered in neuron modeling. Models that treat these aspects of ionic conductances, known as

conductance-based models, can reproduce the rich and complex dynamics of real neurons quite accurately. In this chapter, we discuss both single- and multi-compartment conductance-based models, beginning with the single-compartment case.

membrane potential equation

To review from chapter 5, the membrane potential of a single-compartment neuron model, V, is determined by integrating the equation

$$c_{\rm m}\frac{dV}{dt} = -i_{\rm m} + \frac{I_{\rm e}}{A}\,, \tag{6.1}$$

with $I_{\rm e}$ the electrode current, A the membrane surface area of the cell, and $i_{\rm m}$ the membrane current. In the following subsections, we present expressions for the membrane current in terms of the reversal potentials, maximal conductance parameters, and gating variables of the different conductances of the models being considered. The gating variables and V comprise the dynamic variables of the model. All the gating variables are determined by equations of the form

gating equations

$$\tau_z(V)\frac{dz}{dt} = z_\infty(V) - z\,, \tag{6.2}$$

where z denotes a generic gating variable. The functions $\tau_z(V)$ and $z_\infty(V)$ are determined from experimental data. For some conductances, these are written in terms of the opening and closing rates $\alpha_z(V)$ and $\beta_z(V)$ (see chapter 5), as

$$\tau_z(V) = \frac{1}{\alpha_z(V)+\beta_z(V)} \quad \text{and} \quad z_\infty(V) = \frac{\alpha_z(V)}{\alpha_z(V)+\beta_z(V)}\,. \tag{6.3}$$

We have written $\tau_z(V)$ and $z_\infty(V)$ as functions of the membrane potential, but for Ca^{2+}-dependent currents they also depend on the internal Ca^{2+} concentration. We call $\alpha_z(V)$, $\beta_z(V)$, $\tau_z(V)$, and $z_\infty(V)$ gating functions. A method for numerically integrating equations 6.1 and 6.2 is described in the appendices of chapter 5.

In the following subsections, some basic features of conductance-based models are presented in a sequence of examples of increasing complexity. We do this to illustrate the effects of various conductances and combinations of conductances on neuronal activity. Different cells (and even the same cell held at different resting potentials) can have quite different response properties due to their particular combinations of conductances. Research on conductance-based models focuses on understanding how neuronal response dynamics arises from the properties of membrane and synaptic conductances, and how the characteristics of different neurons interact when they are coupled in networks.

The Connor-Stevens Model

The Hodgkin-Huxley model of action-potential generation, discussed in chapter 5, was developed on the basis of data from the giant axon of the

squid, and we present a multi-compartment simulation of action-potential propagation using this model in a later section. The Connor-Stevens model (Connor and Stevens, 1971; Connor et al. 1977) provides an alternative description of action-potential generation. Like the Hodgkin-Huxley model, it contains fast Na^+, delayed-rectifier K^+, and leakage conductances. The fast Na^+ and delayed-rectifier K^+ conductances have properties somewhat different from those of the Hodgkin-Huxley model, in particular faster kinetics, so the action potentials are briefer. In addition, the Connor-Stevens model contains an extra K^+ conductance, called the A-current, that is transient. K^+ conductances come in wide variety of different forms, and the Connor-Stevens model involves two of them.

A-type potassium current

The membrane current in the Connor-Stevens model is

$$i_m = \overline{g}_L(V - E_L) + \overline{g}_{Na} m^3 h(V - E_{Na}) + \overline{g}_K n^4 (V - E_K) + \overline{g}_A a^3 b(V - E_A)\,, \tag{6.4}$$

where $\overline{g}_L = 0.003$ mS/mm^2 and E_L = -17 mV are the maximal conductance and reversal potential for the leak conductance; and $\overline{g}_{Na} = 1.2$ mS/mm^2, $\overline{g}_K = 0.2$ mS/mm^2, $\overline{g}_A = 0.477$ mS/mm^2, E_{Na} = 55 mV, E_K = -72 mV, and E_A = -75 mV (although the A-current is carried by K^+, the model does not require $E_A = E_K$). The gating variables, m, h, n, a, and b, are determined by equations of the form 6.2 with the gating functions given in appendix A.

The fast Na^+ and delayed-rectifier K^+ conductances generate action potentials in the Connor-Stevens model just as they do in the Hodgkin-Huxley model (see chapter 5). What is the role of the additional A-current? Figure 6.1 illustrates action-potential generation in the Connor-Stevens model. In the absence of an injected electrode current or synaptic input, the membrane potential of the model remains constant at a resting value of -68 mV. For a constant electrode current greater than a threshold value, the model neuron generates action potentials. Figure 6.1A shows how the firing rate of the model depends on the magnitude of the electrode current relative to the threshold value. The firing rate rises continuously from zero and then increases roughly linearly for currents over the range shown. Figure 6.1B shows an example of action-potential generation for one particular value of the electrode current.

Figure 6.1C shows the firing rate as a function of electrode current for the Connor-Stevens model with the maximal conductance of the A-current set to 0. The leakage conductance and reversal potential have been adjusted to keep the resting potential and membrane resistance the same as in the original model. The firing rate is clearly much higher with the A-current turned off. This is because the deinactivation rate of the A-current limits the rise time of the membrane potential between action potentials. In addition, the transition from no firing for currents less than the threshold value to firing with suprathreshold currents is different when the A-current is eliminated. Without the A-current, the firing rate jumps discontinuously to a nonzero value rather than rising continuously. Neurons with firing rates that rise continuously from 0 as a function of electrode current are

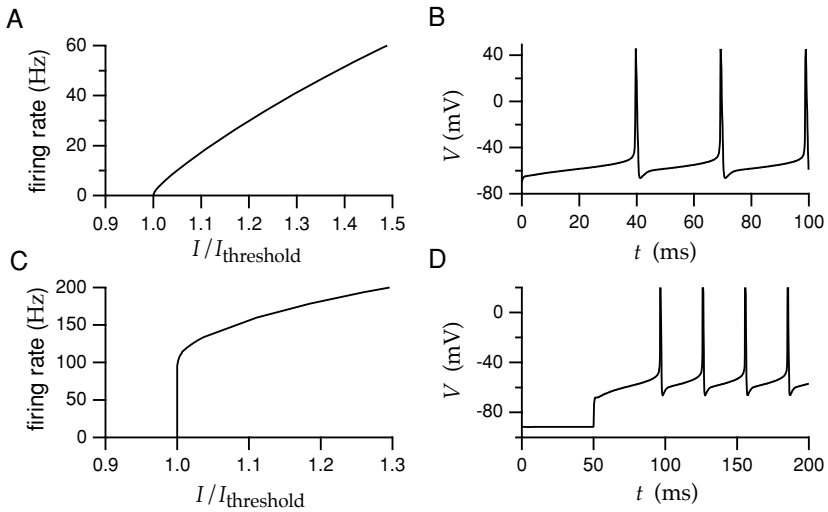

Figure 6.1 Firing of action potentials in the Connor-Stevens model. (A) Firing rate as a function of electrode current. The firing rate rises continuously from 0 as the current increases beyond the threshold value. (B) An example of action potentials generated by constant current injection. (C) Firing rate as a function of electrode current when the A-current is turned off. The firing rate now rises discontinuously from 0 as the current increases beyond the threshold value. (D) Delayed firing due to hyperpolarization. The neuron was held hyperpolarized for a prolonged period by injection of negative current. At $t = 50$ ms, the negative electrode current was switched to a positive value. The A-current delays the occurrence of the first action potential.

type I, type II

called type I, and those with discontinuous jumps in their firing rates at threshold are called type II. An A-current is not the only mechanism that can produce a type I response but, as figures 6.1A and 6.1C show, it plays this role in the Connor-Stevens model. The Hodgkin-Huxley model produces a type II response.

Another effect of the A-current is illustrated in figure 6.1D. Here the model neuron was held hyperpolarized by negative current injection for an extended period of time, and then the current was switched to a positive value. While the neuron was hyperpolarized, the A-current deinactivated, that is, the variable b increased toward 1. When the electrode current switched sign and the neuron depolarized, the A-current first activated and then inactivated. This delayed the first spike following the change in the electrode current.

Postinhibitory Rebound and Bursting

transient Ca^{2+} *conductance*

The range of responses exhibited by the Connor-Stevens model neuron can be extended by including a transient Ca^{2+} conductance. The conductance we use was modeled by Huguenard and McCormick (1992) on the basis of data from thalamic relay cells. The membrane current due to the transient

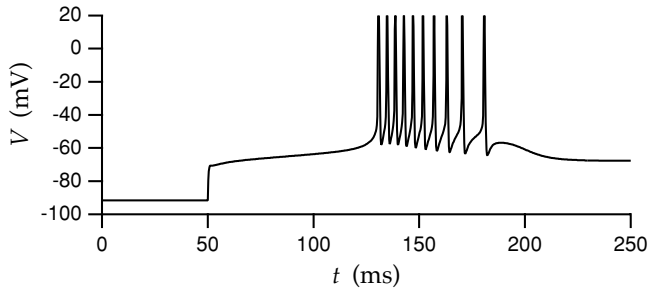

Figure 6.2 A burst of action potentials due to rebound from hyperpolarization. The model neuron was held hyperpolarized for an extended period (until the conductances came to equilibrium) by injection of constant negative electrode current. At $t = 50$ ms, the electrode current was set to 0, and a burst of Na^+ spikes was generated due to an underlying Ca^{2+} spike. The delay in the firing is caused by the presence of the A-current in the model.

Ca^{2+} conductance is expressed as

$$i_{\mathrm{CaT}} = \overline{g}_{\mathrm{CaT}} M^2 H (V - E_{\mathrm{Ca}}) \tag{6.5}$$

with, for the example given here, $\overline{g}_{\mathrm{CaT}} = 0.013$ mS/mm^2 and $E_{\mathrm{Ca}} = 120$ mV. The gating variables for the transient Ca^{2+} conductance are determined from the gating functions in appendix A.

L, T, N and P type Ca^{2+} channels

Several different Ca^{2+} conductances are commonly expressed in neuronal membranes. These are categorized as L, T, N, and P types. L-type Ca^{2+} currents are persistent as far as their voltage dependence is concerned, and they activate at a relatively high threshold. They inactivate due to a Ca^{2+}-dependent rather than voltage-dependent process. T-type Ca^{2+} currents have lower activation thresholds and are transient. N- and P-type Ca^{2+} conductances have intermediate thresholds and are transient and persistent, respectively. They may be responsible for the Ca^{2+} entry that causes the release of transmitter at presynaptic terminals. Entry of Ca^{2+} into a neuron has many secondary consequences ranging from gating Ca^{2+}-dependent channels to inducing long-term modifications of synaptic conductances.

Ca^{2+} spike

burst

A transient Ca^{2+} conductance acts, in many ways, like a slower version of the transient Na^+ conductance that generates action potentials. Instead of producing an action potential, a transient Ca^{2+} conductance generates a slower transient depolarization sometimes called a Ca^{2+} spike. This transient depolarization causes the neuron to fire a burst of action potentials, which are Na^+ spikes riding on the slower Ca^{2+} spike. Figure 6.2 shows such a burst and illustrates one way to produce it. In this example, the model neuron was hyperpolarized for an extended period and then released from hyperpolarization by setting the electrode current to 0. During the prolonged hyperpolarization, the transient Ca^{2+} conductance deinactivated. When the electrode current was set to 0, the resulting depolarization activated the transient Ca^{2+} conductance and generated a burst of

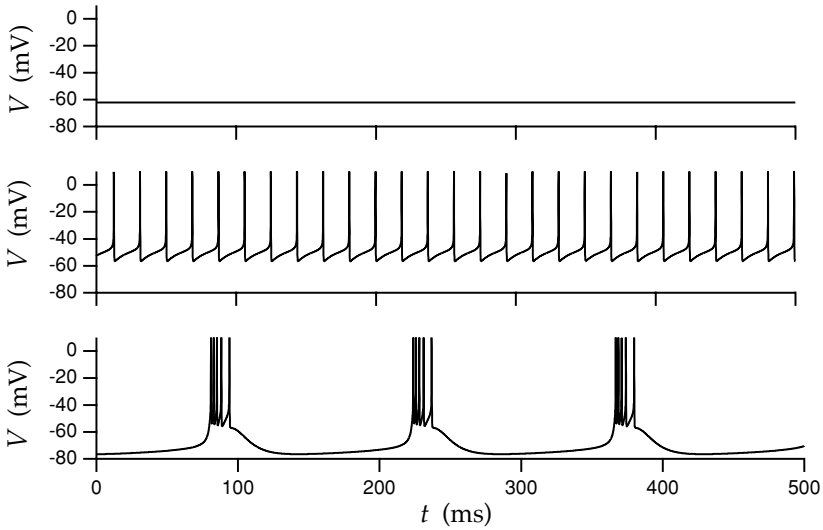

Figure 6.3 Three activity modes of a model thalamic neuron. Upper panel: with no electrode current, the model is silent. Middle panel: when a positive current is injected into the model neuron, it fires action potentials in a regular, periodic pattern. Lower panel: when negative current is injected into the model neuron, it fires action potentials in periodic bursts. (Adapted from Wang, 1994.)

action potentials. The burst in figure 6.2 is delayed due to the presence of the A-current in the Connor-Stevens model to which the Ca^{2+} conductance has been added, and it terminates when the Ca^{2+} conductance inactivates. Generation of action potentials in response to release from hyperpolarization is called postinhibitory rebound because, in a natural setting, the hyperpolarization would be caused by inhibitory synaptic input, not by current injection.

postinhibitory rebound

The transient Ca^{2+} current is an important component of models of thalamic relay neurons. These neurons exhibit different firing patterns in sleep and wakeful states. Action potentials tend to appear in bursts during sleep. Figure 6.3 shows an example of three states of activity of a model thalamic relay cell due to Wang (1994) that has, in addition to fast Na^+, delayed-rectifier K^+, and transient Ca^{2+} conductances, a hyperpolarization-activated mixed-cation conductance and a persistent Na^+ conductance. The cell is silent or fires action potentials in a regular pattern or in bursts, depending on the level of current injection. In particular, injection of small amounts of negative current leads to bursting. This occurs because the hyperpolarization due to the current injection deinactivates the transient Ca^{2+} current and activates the hyperpolarization activated current. The regular firing mode of the middle plot of figure 6.3 is believed to be relevant during wakeful states, when the thalamus is faithfully reporting input from the sensory periphery to the cortex.

thalamic relay neuron

Neurons can fire action potentials either at a steady rate or in bursts even

in the absence of current injection or synaptic input. Periodic bursting is a common feature of neurons in central pattern generators, which are neural circuits that produce periodic patterns of activity to drive rhythmic motor behaviors such as walking, running, or chewing. To illustrate periodic bursting, we consider a model constructed to match the activity of neurons in the crustacean stomatogastric ganglion (STG), a neuronal circuit that controls chewing and digestive rhythms in the foregut of lobsters and crabs. The STG is a model system for investigating the effects of neuromodulators, such as amines and neuropeptides, on the activity patterns of a neural network. Neuromodulators modify neuronal and network behavior by activating, deactivating, or otherwise altering the properties of membrane and synaptic channels. Neuromodulation has a major impact on virtually all neural networks, ranging from peripheral motor pattern generators like the STG to the sensory, motor, and cognitive circuits of the brain.

stomatogastric ganglion

neuromodulator

The model STG neuron contains fast Na^+, delayed-rectifier K^+, A-type K^+, and transient Ca^{2+} conductances similar to those discussed above, although the formulas and parameters used are somewhat different. In addition, the model has a Ca^{2+}-dependent K^+ conductance. Due to the complexity of the model, we do not provide complete descriptions of its conductances except for the Ca^{2+}-dependent K^+ conductance which plays a particularly significant role in the model.

The repolarization of the membrane potential after an action potential is often carried out both by the delayed-rectifier K^+ conductance and by a fast Ca^{2+}-dependent K^+ conductance. Ca^{2+}-dependent K^+ conductances may be voltage dependent, but they are activated primarily by a rise in the level of intracellular Ca^{2+}. A slow Ca^{2+}-dependent K^+ conductance called the after-hyperpolarization (AHP) conductance builds up during sequences of action potentials and typically contributes to the spike-rate adaptation discussed and modeled in chapter 5.

Ca^{2+}*-dependent* K^+ *conductance*

after-hyperpolarization conductance

The Ca^{2+}-dependent K^+ current in the model STG neuron is given by

$$i_{\mathrm{KCa}} = \overline{g}_{\mathrm{KCa}} c^4 (V - E_{\mathrm{K}}) , \tag{6.6}$$

where c obeys an equation of the form 6.2, with c_∞ depending on both the membrane potential and the intracellular Ca^{2+} concentration, $[Ca^{2+}]$ (see appendix A). The intracellular Ca^{2+} concentration is computed in this model using a simplified description in which rises in intracellular Ca^{2+} are caused by influx through membrane Ca^{2+} channels, and Ca^{2+} removal is described by an exponential process. The resulting equation for the intracellular Ca^{2+} concentration, $[Ca^{2+}]$, is

$$\frac{d[\mathrm{Ca}^{2+}]}{dt} = -\gamma i_{\mathrm{Ca}} - \frac{[\mathrm{Ca}^{2+}]}{\tau_{\mathrm{Ca}}} . \tag{6.7}$$

Here i_{Ca} is the total Ca^{2+} current per unit area of membrane, τ_{Ca} is the time constant determining the rate at which intracellular Ca^{2+} is removed, and γ is a factor that converts from the electric current due to Ca^{2+} ion flow

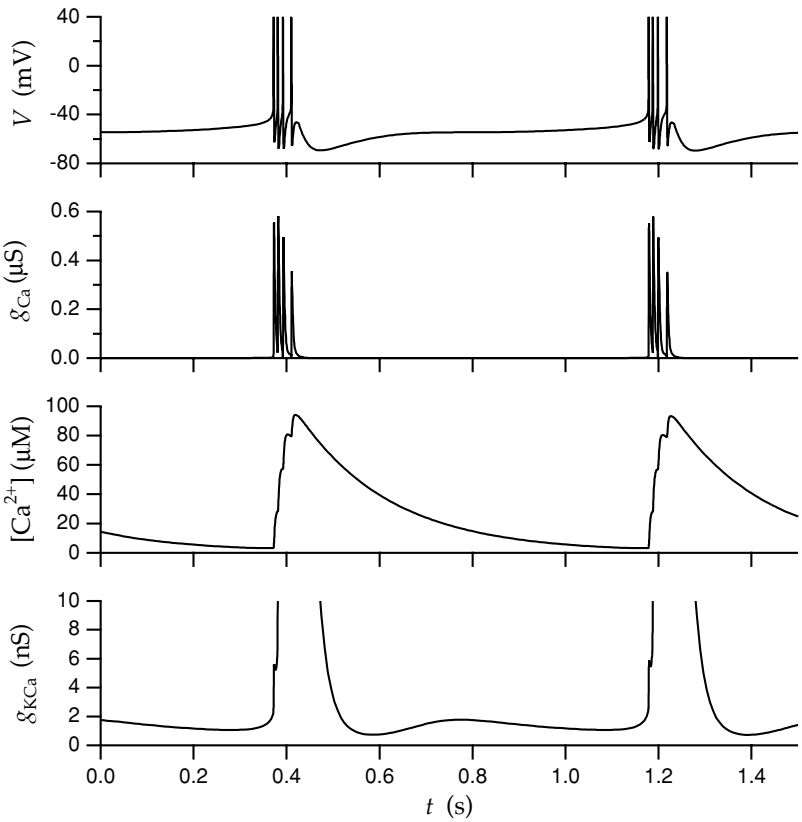

Figure 6.4 Periodic bursting in a model STG neuron. From the top, the panels show the membrane potential, the Ca^{2+} conductance, the intracellular Ca^{2+} concentration, and the Ca^{2+}-dependent K^+ conductance. The Ca^{2+}-dependent K^+ conductance is shown at an expanded scale so the reduction of the conductance due to the falling intracellular Ca^{2+} concentration during the interburst intervals can be seen. In this example, $\tau_{Ca} = 200$ ms. (Simulation by M. Goldman based on a variant of a model of Turrigiano et al., 1995, due to Z. Liu and M. Goldman.)

to the rate at which the Ca^{2+} ion concentration changes within the cell. Because the Ca^{2+} concentration is determined by dividing the number of Ca^{2+} ions in a cell by the total cellular volume and the Ca^{2+} influx is computed by multiplying i_{Ca} by the membrane surface area, γ is proportional to the surface-to-volume ratio for the cell. It also contains a factor that converts from coulombs per second of electrical current to moles per second of Ca^{2+} ions. This factor is $1/(zF)$, where z is the number of charges on the ion ($z = 2$ for Ca^{2+}) and F is the Faraday constant. If, as is normally the case, $[Ca^{2+}]$ is in mols/liter, γ should also contain a factor that converts the volume measure to liters, 10^6 mm^3/liter. Finally, γ is sometimes multiplied by an additional factor that reflects fast intracellular Ca^{2+} buffering. Most of the Ca^{2+} ions that enter a neuron are rapidly bound to intracellular buffers, so only a fraction of the Ca^{2+} current through membrane channels is actually available to change the concentration $[Ca^{2+}]$ of free Ca^{2+} ions

in the cell. This factor is a few percent. The minus sign in front of the γ in equation 6.7 is due to the definition of membrane currents as positive in the outward direction.

Figure 6.4 shows the model STG neuron firing action potentials in bursts. As in the models of figures 6.2 and 6.3, the bursts are transient Ca^{2+} spikes with action potentials riding on top of them. The Ca^{2+} current during these bursts causes a dramatic increase in the intracellular Ca^{2+} concentration. This activates the Ca^{2+}-dependent K^+ current, which, along with the inactivation of the Ca^{2+} current, terminates the burst. The interburst interval is determined primarily by the time it takes for the intracellular Ca^{2+} concentration to return to a low value, which deactivates the Ca^{2+}-dependent K^+ current, allowing another burst to be generated. Although figure 6.4 shows that the conductance of the Ca^{2+}-dependent K^+ current reaches a low value immediately after each burst (due to its voltage dependence), this initial dip is too early for another burst to be generated at that point in the cycle.

6.3 The Cable Equation

Single-compartment models describe the membrane potential over an entire neuron with a single variable. Membrane potentials can vary considerably over the surface of the cell membrane, especially for neurons with long and narrow processes, or if we consider rapidly changing membrane potentials. Figure 6.5A shows the delay and attenuation of an action potential as it propagates from the soma out to the dendrites of a cortical pyramidal neuron. Figure 6.5B shows the delay and attenuation of an excitatory postsynaptic potential (EPSP) initiated in the dendrite by synaptic input as it spreads to the soma. Understanding these features is crucial for determining whether and when a given synaptic input will cause a neuron to fire an action potential.

The attenuation and delay within a neuron are most severe when electrical signals travel down the long, narrow, cablelike structures of dendritic or axonal branches. For this reason, the mathematical analysis of signal propagation within neurons is called cable theory. Dendritic and axonal cables are typically narrow enough that variations of the potential in the radial or axial directions are negligible compared to longitudinal variations. Therefore, the membrane potential along a neuronal cable is expressed as a function of a single longitudinal spatial coordinate x and time, $V(x, t)$, and the basic problem is to solve for this potential.

cable theory

Current flows within a neuron due to voltage gradients. In chapter 5, we discussed how the potential difference across a segment of neuronal cable is related to the longitudinal current flowing down the cable. The longitudinal resistance of a cable segment of length Δx and radius a is given by multiplying the intracellular resistivity r_L by Δx and dividing by the cross-sectional area, πa^2, so that $R_L = r_L \Delta x/(\pi a^2)$. The voltage drop across this

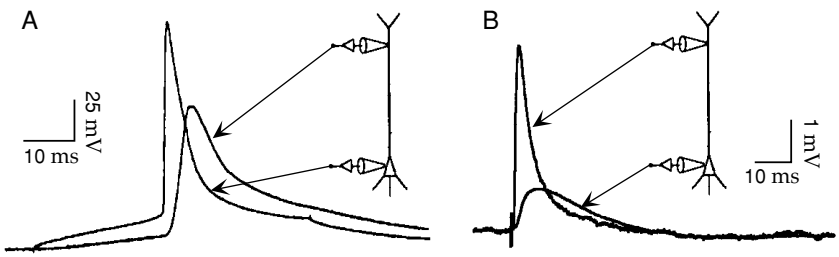

Figure 6.5 Simultaneous intracellular recordings from the soma and apical dendrite of cortical pyramidal neurons in slice preparations. (A) A pulse of current was injected into the soma of the neuron to produce the action potential seen in the somatic recording. The action potential appears delayed and with smaller amplitude in the dendritic recording. (B) A set of axon fibers was stimulated, producing an excitatory synaptic input. The excitatory postsynaptic potential (EPSP) is larger and peaks earlier in the dendrite than in the soma. Note that the scale for the potential is smaller than in A. (A adapted from Stuart and Sakmann, 1994; B adapted from Stuart and Spruston, 1998.)

length of cable, $\Delta V = V(x + \Delta x) - V(x)$, is then related to the amount of longitudinal current flow by Ohm's law. In chapter 5, we discussed the magnitude of this current flow, but for the present purposes, we also need to define a sign convention for its direction. We define currents flowing in the direction of increasing x as positive. By this convention, the relationship between ΔV and I_L given by Ohm's law is $\Delta V = -R_L I_L$ or $\Delta V = -r_L \Delta x I_L/(\pi a^2)$. Solving this for the longitudinal current, we find $I_L = -\pi a^2 \Delta V/(r_L \Delta x)$. It is useful to take the limit of this expression for infinitesimally short cable segments, that is, as $\Delta x \to 0$. In this limit, the ratio of ΔV to Δx becomes the derivative $\partial V/\partial x$. We use a partial derivative here because V can also depend on time. Thus, at any point along a cable of radius a and intracellular resistivity r_L, the longitudinal current flowing in the direction of increasing x is

$$I_L = -\frac{\pi a^2}{r_L}\frac{\partial V}{\partial x}. \tag{6.8}$$

The membrane potential $V(x, t)$ is determined by solving a partial differential equation, the cable equation, that describes how the currents entering, leaving, and flowing within a neuron affect the rate of change of the membrane potential. To derive the cable equation, we consider the currents within the small segment shown in figure 6.6. This segment has a radius a and a short length Δx. The rate of change of the membrane potential due to currents flowing into and out of this region is determined by its capacitance. Recall from chapter 5 that the capacitance of a membrane is determined by multiplying the specific membrane capacitance c_m by the area of the membrane. The cylinder of membrane shown in figure 6.6 has a surface area of $2\pi a \Delta x$, and hence a capacitance of $2\pi a \Delta x c_m$. The amount of current needed to change the membrane potential at a rate $\partial V/\partial t$ is thus $2\pi a \Delta x c_m \partial V/\partial t$.

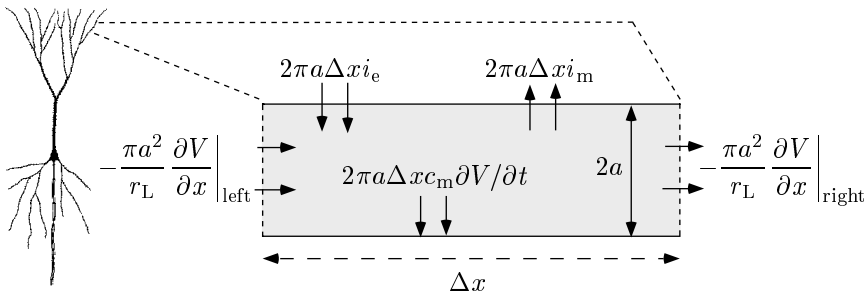

Figure 6.6 The segment of neuron used in the derivation of the cable equation. The longitudinal, membrane, and electrode currents that determine the rate of change of the membrane potential within this segment are denoted. The segment has length Δx and radius a. The expression involving the specific membrane capacitance refers to the rate at which charge builds up on the cell membrane, generating changes in the membrane potential. (The neuron diagram here and in figures 6.15 and 6.16 is from Haberly, 1990.)

All of the currents that can change the membrane potential of the segment being considered are shown in figure 6.6. Current can flow longitudinally into the segment from neighboring segments, and expression 6.8 has been used in figure 6.6 to specify the longitudinal currents at both ends of the segment. Current can flow across the membrane of the segment we are considering through ion and synaptic receptor channels, or through an electrode. The contribution from ion and synaptic channels is expressed as a current per unit area of membrane i_m times the surface area of the segment, $2\pi a\Delta x$. The electrode current is not normally expressed as a current per unit area, but for the present purposes it is convenient to define i_e to be the total electrode current flowing into a given region of the neuronal cable divided by the surface area of that region. The total amount of electrode current being injected into the cable segment of figure 6.6 is then $i_e 2\pi a\Delta x$. Because the electrode current is normally specified by I_e, not by a current per unit area, all the results we obtain will ultimately be re-expressed in terms of I_e. Following the standard convention, membrane and synaptic currents are defined as positive when they are outward, and electrode currents are defined as positive when they are inward.

The cable equation is derived by setting the sum of all the currents shown in figure 6.6 equal to the current needed to charge the membrane. The total longitudinal current entering the cylinder is the difference between the current flowing in on the left and that flowing out on the right. Thus,

$$2\pi a\Delta x c_m \frac{\partial V}{\partial t} = -\left(\frac{\pi a^2}{r_L}\frac{\partial V}{\partial x}\right)\Big|_{left} + \left(\frac{\pi a^2}{r_L}\frac{\partial V}{\partial x}\right)\Big|_{right} - 2\pi a\Delta x(i_m - i_e)\,. \tag{6.9}$$

Dividing both sides of this equation by $2\pi a\Delta x$, we note that the right side involves the term

$$\frac{1}{\Delta x}\left[\left(\frac{\pi a^2}{r_L}\frac{\partial V}{\partial x}\right)\Big|_{right} - \left(\frac{\pi a^2}{r_L}\frac{\partial V}{\partial x}\right)\Big|_{left}\right] \to \frac{\partial}{\partial x}\left(\frac{\pi a^2}{r_L}\frac{\partial V}{\partial x}\right). \tag{6.10}$$

The arrow refers to the limit $\Delta x \to 0$, which we now take. We can move r_L outside the derivative in this equation under the assumption that it is not a function of position. However, the factor of a^2 must remain inside the derivative unless it is independent of x. Substituting the result 6.10 into 6.9, we obtain the cable equation,

cable equation

$$c_m \frac{\partial V}{\partial t} = \frac{1}{2ar_L} \frac{\partial}{\partial x}\left(a^2 \frac{\partial V}{\partial x}\right) - i_m + i_e \,. \tag{6.11}$$

boundary conditions for the cable equation

To determine the membrane potential, equation (6.11) must be augmented by appropriate boundary conditions. The boundary conditions specify what happens to the membrane potential when the neuronal cable branches or terminates. The point at which a cable branches, or equivalently where multiple cable segments join, is called a node. At such a branching node, the potential must be continuous, that is, the functions $V(x, t)$ defined along each of the segments must yield the same result when evaluated at the x value corresponding to the node. In addition, charge must be conserved, which means that the sum of the longitudinal currents entering (or leaving) a node along all of its branches must be 0. According to equation 6.8, the longitudinal current entering a node is proportional to the square of the cable radius times the derivative of the potential evaluated at that point, $a^2 \partial V/\partial x$. The sum of the longitudinal currents entering the node, computed by evaluating these derivatives along each cable segment at the point where they meet at the node, must be 0.

Several different boundary conditions can be imposed at the end of a terminating cable segment. One simple condition is that no current flows out of the end of the cable. By equation 6.8, this means that the spatial derivative of the potential must vanish at a termination point.

Due to the complexities of neuronal membrane currents and morphologies, the cable equation is most often solved numerically, using multicompartmental techniques described later in this chapter. However, it is useful to study analytic solutions of the cable equation in simple cases to get a feel for how different morphological features, such as long dendritic cables, branching nodes, changes in cable radii, and cable ends, affect the membrane potential.

Linear Cable Theory

Before we can solve the cable equation by any method, the membrane current i_m must be specified. We discussed models of various ion channel contributions to the membrane current in chapter 5 and earlier in this chapter. These models typically produce nonlinear expressions that are too complex to allow analytic solution of the cable equation. The analytic solutions we discuss use two rather drastic approximations: synaptic currents are ignored, and the membrane current is written as a linear function of the

membrane potential. Eliminating synaptic currents requires us to examine how a neuron responds to the electrode current i_e. In some cases, electrode current can mimic the effects of a synaptic conductance, although the two are not equivalent. In any case, studying responses to electrode current allows us to investigate the effects of different morphologies on membrane potentials.

Typically, a linear approximation for the membrane current is valid only if the membrane potential stays within a limited range, for example, close to the resting potential of the cell. The resting potential is defined as the potential where no net current flows across the membrane. Near this potential, we approximate the membrane current per unit area as

$$i_m = (V - V_{rest})/r_m\,, \tag{6.12}$$

where V_{rest} is the resting potential and r_m is the specific membrane resistance. It is convenient to define v as the membrane potential relative to the resting potential, $v = V - V_{rest}$, so that $i_m = v/r_m$.

$v = V - V_{rest}$

If the radii of the cable segments used to model a neuron are constant except at branches and abrupt junctions, the factor a^2 in equation 6.11 can be taken out of the derivative and combined with the prefactor $1/2ar_L$ to produce a factor $a/2r_L$ that multiplies the spatial second derivative. With this modification and use of the linear expression for the membrane current, the cable equation for v is

$$c_m\frac{\partial v}{\partial t} = \frac{a}{2r_L}\frac{\partial^2 v}{\partial x^2} - \frac{v}{r_m} + i_e\,. \tag{6.13}$$

It is convenient to multiply this equation by r_m, turning the factor that multiplies the time derivative on the left side into the membrane time constant $\tau_m = r_m c_m$. This also changes the expression multiplying the spatial second derivative on the right side of equation 6.13 to $ar_m/2r_L$. This factor has the dimensions of length squared, and it defines a fundamental length constant for a segment of cable of radius a, the electrotonic length,

electrotonic length λ

$$\lambda = \sqrt{\frac{ar_m}{2r_L}}\,. \tag{6.14}$$

Using the values $r_m = 1\ \mathrm{M\Omega\cdot mm^2}$ and $r_L = 1\ \mathrm{k\Omega\cdot mm}$, a cable of radius $a = 2\ \mu\mathrm{m}$ has an electrotonic length of 1 mm. A segment of cable with radius a and length λ has a membrane resistance that is equal to its longitudinal resistance, as can be seen from equation 6.14,

R_λ

$$R_\lambda = \frac{r_m}{2\pi a\lambda} = \frac{r_L\lambda}{\pi a^2}\,. \tag{6.15}$$

The resistance R_λ defined by this equation is a useful quantity that enters into a number of calculations.

linear cable equation

Expressed in terms of τ_m and λ, the cable equation becomes

$$\tau_m\frac{\partial v}{\partial t} = \lambda^2\frac{\partial^2 v}{\partial x^2} - v + r_m i_e\,. \tag{6.16}$$

Equation 6.16 is a linear equation for v similar to the diffusion equation, and it can be solved by standard methods of mathematical analysis. The constants τ_m and λ set the scale for temporal and spatial variations in the membrane potential. For example, the membrane potential requires a time of order τ_m to settle down after a transient, and deviations in the membrane potential due to localized electrode currents decay back to 0 over a length of order λ.

The membrane potential is affected both by the form of the cable equation and by the boundary conditions imposed at branching nodes and terminations. To isolate these two effects, we consider two idealized cases: an infinite cable that does not branch or terminate, and a single branching node that joins three semi-infinite cables. Of course, real neuronal cables are not infinitely long, but the solutions we find are applicable for long cables far from their ends. We determine the potential for both of these morphologies when current is injected at a single point. Because the equation we are studying is linear, the membrane potential for any other spatial distribution of electrode current can be determined by summing solutions corresponding to current injection at different points. The use of point injection to build more general solutions is a standard method of linear analysis. In this context, the solution for a point source of current injection is called a Green's function.

Green's function

An Infinite Cable

In general, solutions to the linear cable equation are functions of both position and time. However, if the current being injected is held constant, the membrane potential settles to a steady-state solution that is independent of time. Solving for this time-independent solution is easier than solving the full time-dependent equation, because the cable equation reduces to an ordinary differential equation in the static case,

$$\lambda^2 \frac{d^2 v}{dx^2} = v - r_m i_e \,. \tag{6.17}$$

For the localized current injection we wish to study, i_e is 0 everywhere except within a small region of size Δx around the injection site, which we take to be $x = 0$. Eventually we will let $\Delta x \to 0$. Away from the injection site, the linear cable equation is $\lambda^2 d^2 v/dx^2 = v$, which has the general solution $v(x) = B_1 \exp(-x/\lambda) + B_2 \exp(x/\lambda)$ with as yet undetermined coefficients B_1 and B_2. These constant coefficients are determined by imposing boundary conditions appropriate to the particular morphology being considered. For an infinite cable, on physical grounds we simply require that the solution does not grow without bound when $x \to \pm\infty$. This means that we must choose the solution with $B_1 = 0$ for the region $x < 0$ and the solution with $B_2 = 0$ for $x > 0$. Because the solution must be continuous at $x = 0$, we must require $B_1 = B_2 = B$, and these two solutions can be combined into a single expression, $v(x) = B \exp(-|x|/\lambda)$. The remaining task

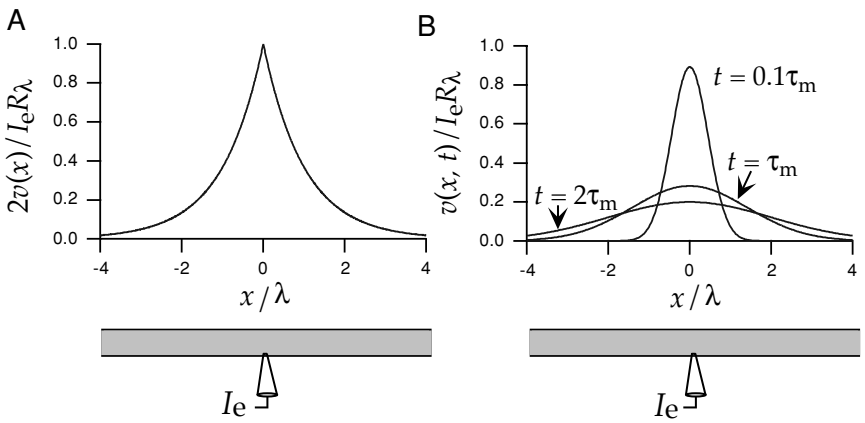

Figure 6.7 The potential for current injection at the point $x = 0$ along an infinite cable. (A) Static solution for a constant electrode current. The potential decays exponentially away from the site of current injection. (B) Time-dependent solution for a δ function pulse of current. The potential is described by a Gaussian function centered at the site of current injection that broadens and shrinks in amplitude over time.

is to determine B, which we do by balancing the current injected with the current that diffuses away from $x = 0$.

In the small region of size Δx around $x = 0$ where the current is injected, the full equation $\lambda^2 d^2v/dx^2 = v - r_m i_e$ must be solved. If the total amount of current injected by the electrode is I_e, the current per unit area injected into this region is $I_e/(2\pi a \Delta x)$. This grows without bound as $\Delta x \to 0$. The first derivative of the membrane potential $v(x) = B\exp(-|x|/\lambda)$ is discontinuous at the point $x = 0$. For small Δx, the derivative at one side of the region we are discussing (at $x = -\Delta x/2$) is approximately B/λ, while at the other side (at $x = +\Delta x/2$) it is $-B/\lambda$. In these expressions, we have used the fact that Δx is small to set $\exp(-|\Delta x|/2\lambda) \approx 1$. For small Δx, the second derivative is approximately the difference between these two first derivatives divided by Δx, which is $-2B/(\lambda \Delta x)$. We can ignore the term v in the cable equation within this small region, because it is not proportional to $1/\Delta x$. Substituting the expressions we have derived for the remaining terms in the equation, we find that $-2\lambda^2 B/(\lambda \Delta x) = -r_m I_e/(2\pi a \Delta x)$, which means that $B = I_e R_\lambda/2$, using R_λ from equation 6.15. Thus, the membrane potential for static current injection at the point $x = 0$ along an infinite cable is

$$v(x) = \frac{I_e R_\lambda}{2} \exp\left(-\frac{|x|}{\lambda}\right). \tag{6.18}$$

According to this result, the membrane potential away from the site of current injection ($x = 0$) decays exponentially with length constant λ (see figure 6.7A). The ratio of the membrane potential at the injection site to the magnitude of the injected current is called the input resistance of the cable. The value of the potential at $x = 0$ is $I_e R_\lambda/2$, indicating that the

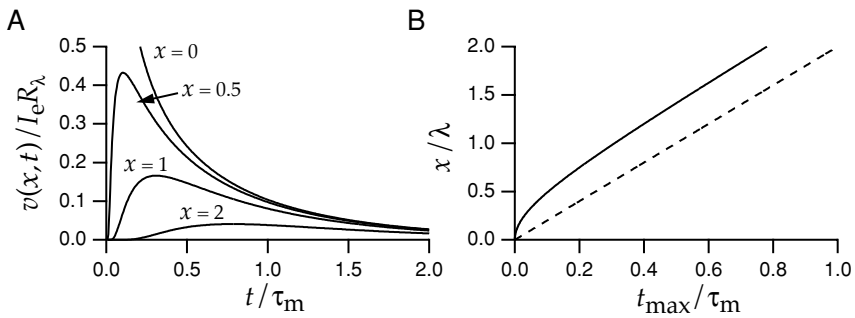

Figure 6.8 Time dependence of the potential on an infinite cable in response to a pulse of current injected at the point $x=0$ at time $t=0$. (A) The potential is always largest at the site of current injection. At any fixed point, it reaches its maximum value as a function of time later for measurement sites located farther away from the current source. (B) Movement of the temporal maximum of the potential. The solid line shows the relationship between the measurement location x and the time t_{max} when the potential reaches its maximum value at that location. The dashed line corresponds to a constant velocity $2\lambda/\tau_m$.

infinite cable has an input resistance of $R_\lambda/2$. Each direction of the cable acts like a resistance of R_λ, and these two act in parallel to produce a total resistance half as big. Note that each semi-infinite cable extending from the point $x = 0$ has a resistance equal to a finite cable of length λ.

We now consider the membrane potential produced by an instantaneous pulse of current injected at the point $x = 0$ at the time $t = 0$. Specifically, we consider $i_e = I_e\tau_m\delta(x)\delta(t)/2\pi a$, which means that the current pulse delivers a total charge of $I_e\tau_m$. We do not derive the solution for this case (see Tuckwell, 1988, for example), but simply state the answer,

$$v(x,t) = \frac{I_e R_\lambda}{\sqrt{4\pi t/\tau_m}} \exp\left(-\frac{\tau_m x^2}{4\lambda^2 t}\right) \exp\left(-\frac{t}{\tau_m}\right). \qquad (6.19)$$

In this case, the spatial dependence of the potential is determined by a Gaussian, rather than an exponential function. The Gaussian is always centered around the injection site, so the potential is always largest at $x = 0$. The width of the Gaussian curve around $x = 0$ is proportional to $\lambda\sqrt{t/\tau_m}$. As expected, λ sets the scale for this spatial variation, but the width also grows as the square root of the time measured in units of τ_m. The factor $(4\pi t/\tau_m)^{-1/2}$ in equation 6.19 preserves the total area under this Gaussian curve, but the additional exponential factor $\exp(-t/\tau_m)$ reduces the integrated amplitude over time. As a result, the spatial dependence of the membrane potential is described by a spreading Gaussian function with an integral that decays exponentially (figure 6.7B).

Figure 6.8 shows the solution of equation 6.19 plotted at various fixed positions as a function of time. Figure 6.8A shows that the membrane potential measured farther from the injection site reaches its maximum value at later times. It is important to keep in mind that the membrane potential spreads out from the region $x = 0$; it does not propagate like a wave. Nevertheless,

we can define a type of "velocity" for this solution by computing the time $t_{\max}$ when the maximum of the potential occurs at a given spatial location. This is done by setting the time derivative of $v(x,t)$ in equation 6.19 to 0, giving

$$t_{\max} = \frac{\tau_m}{4}\left(\sqrt{1+4(x/\lambda)^2}-1\right). \tag{6.20}$$

For large x, $t_{\max} \approx x\tau_m/2\lambda$, corresponding to a velocity of $2\lambda/\tau_m$. For smaller x values, the location of the maximum moves faster than this "velocity" would imply (figure 6.8B).

An Isolated Branching Node

To illustrate the effects of branching on the membrane potential in response to a point source of current injection, we consider a single isolated junction of three semi-infinite cables, as shown in the bottom panels of figure 6.9. For simplicity, we discuss the solution for static current injection at a point, but the results generalize directly to the case of time-dependent currents. We label the potentials along the three segments v_1, v_2, and v_3, and label the distance outward from the junction point along any given segment by the coordinate x (although in figure 6.9 a slightly different convention is used). The electrode injection site is located a distance y away from the junction along segment 2. The solution for the three segments is then

$$\begin{aligned} v_1(x) &= p_1 I_e R_{\lambda_1} \exp(-x/\lambda_1 - y/\lambda_2) \\ v_2(x) &= \frac{I_e R_{\lambda_2}}{2}\left[\exp(-|y-x|/\lambda_2) + (2p_2-1)\exp(-(y+x)/\lambda_2)\right] \\ v_3(x) &= p_3 I_e R_{\lambda_3} \exp(-x/\lambda_3 - y/\lambda_2), \end{aligned} \tag{6.21}$$

where, for $i = 1$, 2, and 3,

$$p_i = \frac{a_i^{3/2}}{a_1^{3/2}+a_2^{3/2}+a_3^{3/2}} \quad , \quad \lambda_i = \sqrt{\frac{a_i r_m}{2r_L}} \text{ , and } R_{\lambda_i} = \frac{r_L \lambda_i}{\pi a_i^2}. \tag{6.22}$$

Note that the distances x and y appearing in the exponential functions are divided by the electrotonic length of the segment along which the potential is measured or the current is injected. This solution satisfies the cable equation, because it is constructed by combining solutions of the form 6.18. The only term that has a discontinuous first derivative within the range being considered is the first term in the expression for v_2, and this solves the cable equation at the current injection site because it is identical to 6.18. We leave it to the reader to verify that this solution satisfies the boundary conditions $v_1(0) = v_2(0) = v_3(0)$ and $\sum a_i^2 \partial v_i/\partial x = 0$.

Figure 6.9 shows the potential near a junction where a cable of radius 2 μ breaks into two thinner cables of radius 1 μ. In figure 6.9A, current is injected along the thicker cable, and in figure 6.9B it is injected along one

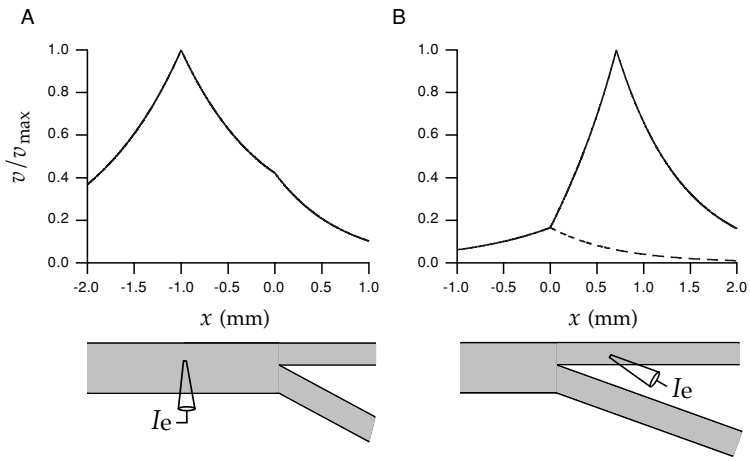

Figure 6.9 The potentials along the three branches of an isolated junction for a current injection site one electrotonic length constant away from the junction. The potential v is plotted relative to $v_{\max}$, which is v at the site of the electrode. The thick branch has a radius of 2 μ and an electrotonic length constant $\lambda = 1$ mm, and the two thin branches have radii of 1 μ and $\lambda = 2^{-1/2}$ mm. (A) Current injection along the thick branch. The potentials along both of the thin branches, shown by the solid curve over the range $x > 0$, are identical. The solid curve over the range $x < 0$ shows the potential on the thick branch where current is being injected. (B) Current injection along one of the thin branches. The dashed line shows the potential along the thin branch where current injection does not occur. The solid line shows the potential along the thick branch for $x < 0$ and along the thin branch receiving the injected current for $x > 0$.

of the thinner branches. In both cases, the site of current injection is one electrotonic length constant away from the junction. The two daughter branches have little effect on the falloff of the potential away from the electrode site in figure 6.9A. This is because the thin branches do not represent a large current sink. The thick branch has a bigger effect on the attenuation of the potential along the thin branch receiving the electrode current in figure 6.9B. This can be seen as an asymmetry in the falloff of the potential on either side of the electrode. Loading by the thick cable segment contributes to a quite severe attenuation between the two thin branches in figure 6.9B. Comparison of figures 6.9A and B reveals a general feature of static attenuation in a passive cable: attenuation near the soma due to potentials arising in the periphery is typically greater than attenuation in the periphery due to potentials arising near the soma.

The Rall Model

The infinite and semi-infinite cables we have considered are clearly mathematical idealizations. We now turn to a model neuron introduced by Rall (1959, 1977) that, though still highly simplified, captures some of the important elements that affect the responses of real neurons. Most neurons receive their synaptic inputs over complex dendritic trees. The integrated

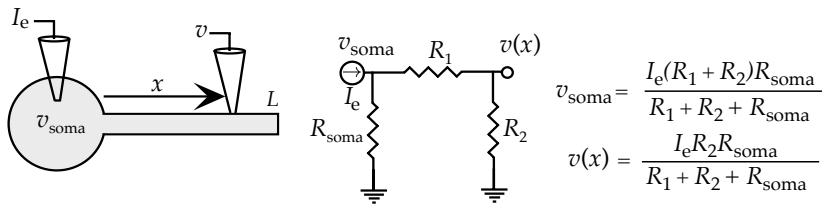

Figure 6.10 The Rall model with static current injected into the soma. The schematic at left shows the recording setup. The potential is measured at the soma and at a distance x along the equivalent cable. The central diagram is the equivalent circuit for this case, and the corresponding formulas for the somatic and dendritic voltages are given at the right. The symbols at the bottom of the resistances R_{soma} and R_2 indicate that $v = 0$ at these points. R_{soma} is the membrane resistance of the soma, and R_1 and R_2 are the resistances given in equations 6.23 and 6.24.

effect of these inputs is usually measured from the soma, and the spike-initiation region of the axon that determines whether the neuron fires an action potential is typically located near the soma. In Rall's model, a compact soma region (represented by one compartment) is connected to a single equivalent cylindrical cable that replaces the entire dendritic region of the neuron (see the schematics in figures 6.10 and 6.12). The critical feature of the model is the choice of the radius and length for the equivalent cable to best match the properties of the dendritic structure being approximated.

The radius a and length L of the equivalent cable are determined by matching two important elements of the full dendritic tree. These are its average length in electrotonic units, which determines the amount of attenuation, and the total surface area, which determines the total membrane resistance and capacitance. The average electrotonic length of a dendrite is determined by considering direct paths from the soma to the terminals of the dendrite. The electrotonic lengths for these paths are constructed by measuring the distance traveled along each of the cable segments traversed in units of the electrotonic length constant for that segment. In general, the total electrotonic length measured by summing these electrotonic segment lengths depends on which terminal of the tree is used as the end point. However, an average value can be used to define an electrotonic length for the full dendritic structure. The length L of the equivalent cable is then chosen so that L/λ is equal to this average electrotonic length, where λ is the length constant for the equivalent cable. The radius of the equivalent cable, which is needed to compute λ, is determined by setting the surface area of the equivalent cable, $2\pi aL$, equal to the surface area of the full dendritic tree.

Under some restrictive circumstances the equivalent cable reproduces the effects of a full tree exactly. Among these conditions is the requirement $a_1^{3/2} = a_2^{3/2} + a_3^{3/2}$ on the radii of any three segments being joined at a node within the tree. Note from equation 6.22 that this condition makes $p_1 = p_2 + p_3 = 1/2$. However, even when the so-called $3/2$ law is not exact, the equivalent cable is an extremely useful and often reasonably accurate simplification.

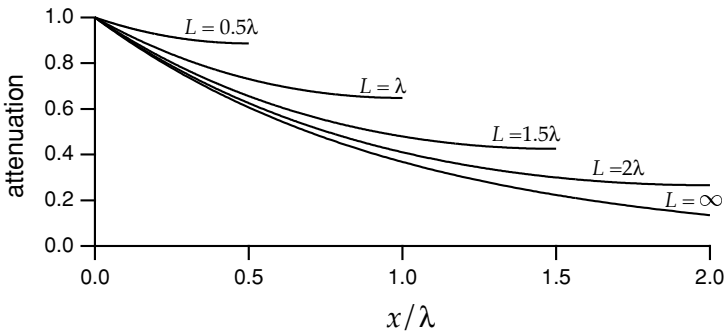

Figure 6.11 Voltage and current attenuation for the Rall model. The attenuation plotted is the ratio of the dendritic voltage to the somatic voltage for the recording setup of figure 6.10, or the ratio of the somatic current to the electrode current for the arrangement in figure 6.12. Attenuation is plotted as a function of x/λ for different equivalent cable lengths.

Figures 6.10 and 6.12 depict static solutions of the Rall model for two different recording configurations, expressed in the form of equivalent circuits. The equivalent circuits are an intuitive way of describing the solution of the cable equation. In figure 6.10, constant current is injected into the soma. The circuit diagram shows an arrangement of resistors that replicates the results of solving the time-independent cable equation (equation 6.17) for the purposes of voltage measurements at the soma, v_{soma}, and at a distance x along the equivalent cable, $v(x)$. The values for these resistances (and similarly the values of R_3 and R_4 given below) are set so that the equivalent circuit reconstructs the solution of the cable equation obtained using standard methods (see, for example, Tuckwell, 1988). R_{soma} is the membrane resistance of the soma, and

$$R_1 = \frac{R_\lambda \left(\cosh\left(L/\lambda\right) - \cosh\left((L-x)/\lambda\right)\right)}{\sinh\left(L/\lambda\right)} \tag{6.23}$$

$$R_2 = \frac{R_\lambda \cosh\left((L-x)/\lambda\right)}{\sinh\left(L/\lambda\right)}. \tag{6.24}$$

Expressions for v_{soma} and $v(x)$, arising directly from the equivalent circuit using standard rules of circuit analysis (see the Mathematical Appendix), are given at the right side of figure 6.10.

The input resistance of the Rall model neuron, as measured from the soma, is determined by the somatic resistance R_{soma} acting in parallel with the effective resistance of the cable, and is $(R_1 + R_2)R_{\text{soma}}/(R_1 + R_2 + R_{\text{soma}})$. The effective resistance of the cable, $R_1 + R_2 = R_\lambda/\tanh(L)$, approaches the value R_λ when $L \gg \lambda$. The effect of lengthening a cable saturates when it gets much longer than its electrotonic length. The voltage attenuation caused by the cable is defined as the ratio of the dendritic potential to the somatic potential, and in this case it is given by

$$\frac{v(x)}{v_{\text{soma}}} = \frac{R_2}{R_1 + R_2} = \frac{\cosh\left((L-x)/\lambda\right)}{\cosh\left(L/\lambda\right)}. \tag{6.25}$$

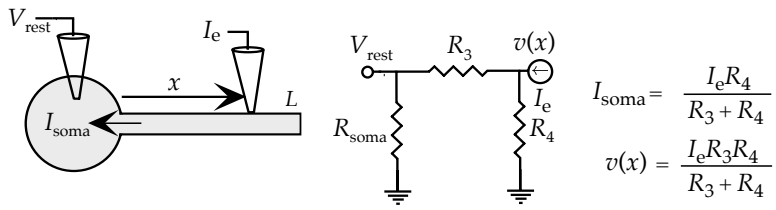

Figure 6.12 The Rall model with static current injected a distance x along the equivalent cable while the soma is clamped at its resting potential. The schematic at left shows the recording setup. The potential at the site of the current injection and the current entering the soma are measured. The central diagram is the equivalent circuit for this case, and the corresponding formulas for the somatic current and dendritic voltage are given at the right. R_{soma} is the membrane resistance of the soma, and R_3 and R_4 are the resistances given in equations 6.26 and 6.27.

This result is plotted in figure 6.11.

Figure 6.12 shows the equivalent circuit for the Rall model when current is injected at a location x along the cable, and the soma is clamped at $v_{soma} = 0$ (or equivalently $V_{soma} = V_{rest}$). The equivalent circuit can be used to determine the current entering the soma and the voltage at the site of current injection. In this case, the somatic resistance is irrelevant because the soma is clamped at its resting potential. The other resistances are

$$R_3 = R_\lambda \sinh(x/\lambda) \tag{6.26}$$

and

$$R_4 = \frac{R_\lambda \sinh(x/\lambda)\cosh((L-x)/\lambda)}{\cosh(L/\lambda) - \cosh((L-x)/\lambda)}. \tag{6.27}$$

The input resistance for this configuration, as measured from the dendrite, is determined by R_3 and R_4 acting in parallel, and is $R_3R_4/(R_3+R_4) = R_\lambda \sinh(x/\lambda)\cosh((L-x)/\lambda)/\cosh(L/\lambda)$. When L and x are both much larger than λ, this approaches the limiting value R_λ. The current attenuation is defined as the ratio of the somatic current to the electrode current, and is given by

$$\frac{I_{soma}}{I_e} = \frac{R_4}{R_3 + R_4} = \frac{\cosh((L-x)/\lambda)}{\cosh(L/\lambda)}. \tag{6.28}$$

The inward current attenuation (plotted in figure 6.11) for the recording configuration of figure 6.12 is identical to the outward voltage attenuation for figure 6.10 given by equation 6.25. Equality of the voltage attenuation measured in one direction and the current attenuation measured in the opposite direction is a general feature of linear cable theory.

The Morphoelectrotonic Transform

The membrane potential for a neuron of complex morphology is obviously much more difficult to compute than the simple cases we have

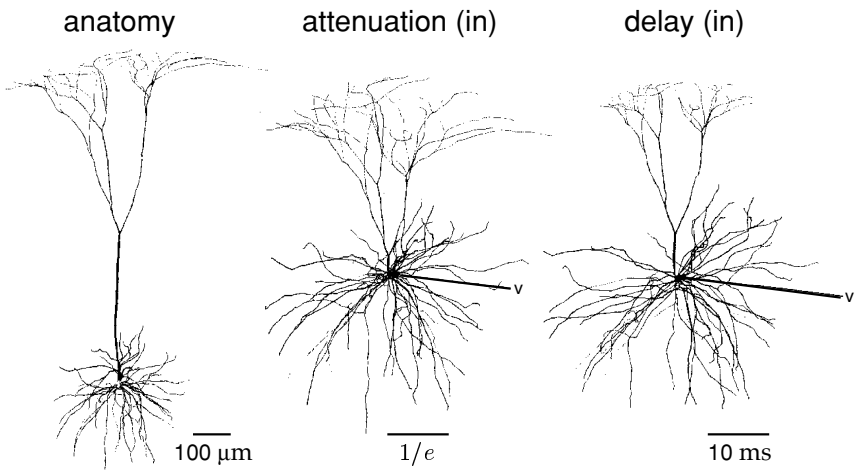

Figure 6.13 The morphoelectrotonic transform of a cortical neuron. The left panel is a normal drawing of the neuron. The central panel is a diagram in which the distance between any point and the soma is proportional to the logarithm of the steady-state attenuation between the soma and that point for static current injected at the terminals of the dendrites. The scale bar denotes the distance corresponding to an attenuation of $\exp(-1)$. In the right panel, the distance from the soma to a given point is proportional to the inward delay, which is the centroid of the soma potential minus the centroid at the periphery when a pulse of current is injected peripherally. The v labels in the diagrams indicate that the reference potential in these cases is the somatic potential. (Adapted from Zador et al, 1995.)

considered. Fortunately, efficient numerical schemes (discussed later in this chapter) exist for generating solutions for complex cable structures. However, even when the solution is known, it is still difficult to visualize the effects of a complex morphology on the potential. Zador et al. (1995; see also Tsai et al., 1994) devised a scheme for depicting the attenuation and delay of the membrane potential for complex morphologies. The voltage attenuation, as plotted in figure 6.11, is not an appropriate quantity to represent geometrically because it is not additive. Consider three points along a cable satisfying $x_1 > x_2 > x_3$. The attenuation between x_1 and x_3 is the product of the attenuation from x_1 to x_2 and from x_2 to x_3, $v(x_1)/v(x_3) = (v(x_1)/v(x_2))(v(x_2)/v(x_3))$. An additive quantity can be obtained by taking the logarithm of the attenuation, due to the identity $\ln(v(x_1)/v(x_3)) = \ln(v(x_1)/v(x_2)) + \ln(v(x_2)/v(x_3))$. The morphoelectrotonic transform is a diagram of a neuron in which the distance between any two points is determined by the logarithm of the ratio of the membrane potentials at these two locations, not by the actual size of the neuron.

morphoelectrotonic transform

Another morphoelectrotonic transform can be used to indicate the amount of delay in the voltage waveform produced by a transient input current. The morphoelectrotonic transform uses a definition of delay different from that used in Figure 6.8B. The delay between any two points is defined as the difference between the centroid, or center of "mass", of the voltage

response at these points. Specifically, the centroid at point x is defined as $\int dt\, tv(x,t) / \int dt\, v(x,t)$. Like the log-attenuation, the delay between any two points on a neuron is represented in the morphoelectrotonic transform as a distance.

Morphoelectrotonic transforms of a pyramidal cell from layer 5 of cat visual cortex are shown in figures 6.13 and 6.14. The left panel of figure 6.13 is a normal drawing of the neuron being studied, the middle panel shows the steady-state attenuation, and the right panel shows the delay. The transformed diagrams correspond to current being injected peripherally, with somatic potentials being compared to dendritic potentials. These figures indicate that, for potentials generated in the periphery, the apical and basal dendrites are much more uniform than the morphology would suggest.

The small neuron diagram at the upper left of figure 6.14 shows attenuation for the reverse situation from figure 6.13, when constant current is injected into the soma and dendritic potentials are compared with the somatic potential. Note how much smaller this diagram is than the one in the central panel of figure 6.13. This illustrates the general feature, mentioned previously, that potentials are attenuated much less in the outward than in the inward direction. This is because the thin dendrites provide less of a current sink for potentials arising from the soma than the soma provides for potentials coming from the dendrites.

The capacitance of neuronal cables causes the voltage attenuation for time-dependent current injection to increase as a function of frequency. Figure 6.14 compares the attenuation of dendritic potentials relative to the somatic potential when constant or sinusoidal current of two different frequencies is injected into the soma. Clearly, attenuation increases dramatically as a function of frequency. Thus, a neuron that appears electrotonically compact for static or low frequency current injection may be not compact when higher frequencies are considered. For example, action potential waveforms, which correspond to frequencies around 500 Hz, are much more severely attenuated within neurons than slower varying potentials.

6.4 Multi-compartment Models

The cable equation can be solved analytically only in relatively simple cases. When the complexities of real membrane conductances are included, the membrane potential must be computed numerically. This is done by splitting the neuron being modeled into separate regions or compartments, and approximating the continuous membrane potential $V(x,t)$ by a discrete set of values representing the potentials within the different compartments. This assumes that each compartment is small enough so that there is negligible variation of the membrane potential across it. The precision of such a multi-compartmental description depends on the

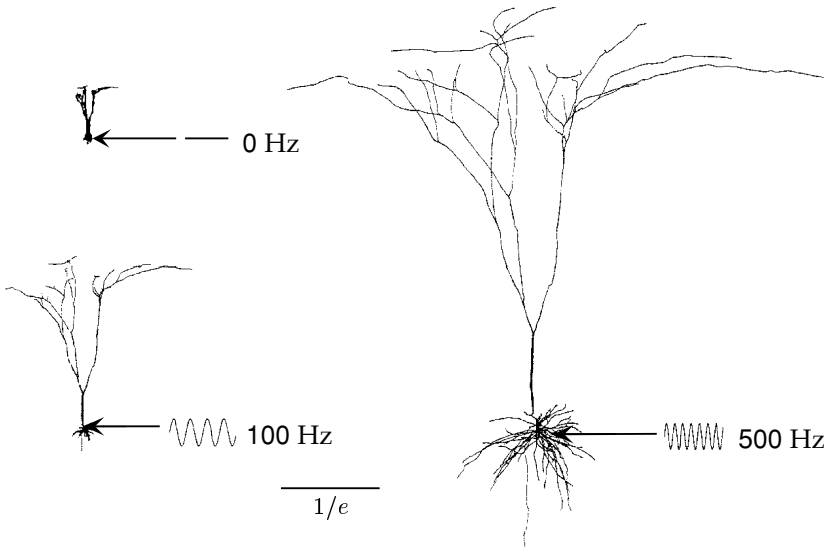

Figure 6.14 Morphoelectrotonic transforms of the same neuron as in figure 6.13 but showing the outward log-attenuation for constant and oscillating input currents. Distances in these diagrams are proportional to the logarithm of the amplitude of the voltage oscillations at a given point divided by the amplitude of the oscillations at the soma when a sinusoidal current is injected into the soma. The upper left panel corresponds to constant current injection, the lower left panel to sinusoidal current injection at a frequency of 100 Hz, and the right panel to an injection frequency of 500 Hz. The scale bar denotes the distance corresponding to an attenuation of $\exp(-1)$. (Adapted from Zador et al., 1995.)

number of compartments used and on their size relative to the length constants that characterize their electrotonic compactness. Figure 6.15 shows a schematic diagram of a cortical pyramidal neuron, along with a series of compartmental approximations of its structure. The number of compartments used can range from thousands, in some models, to one, for the description at the extreme right of figure 6.15.

In a multi-compartment model, each compartment has its own membrane potential V_μ (where μ labels compartments), and its own gating variables that determine the membrane current for compartment μ, $i_{\rm m}^\mu$. Each membrane potential V_μ satisfies an equation similar to 6.1 except that the compartments couple to their neighbors in the multi-compartment structure (figure 6.16). For a nonbranching cable, each compartment is coupled to two neighbors and the equations for the membrane potentials of the compartments are

$$c_{\rm m}\frac{dV_\mu}{dt} = -i_{\rm m}^\mu + \frac{I_{\rm e}^\mu}{A_\mu} + g_{\mu,\mu+1}(V_{\mu+1} - V_\mu) + g_{\mu,\mu-1}(V_{\mu-1} - V_\mu)\,. \quad (6.29)$$

Here $I_{\rm e}^\mu$ is the total electrode current flowing into compartment μ, and A_μ is its surface area. Compartments at the ends of a cable have only one neighbor, and thus only a single term replacing the last two terms in equation 6.29. For a compartment where a cable branches in two, there are

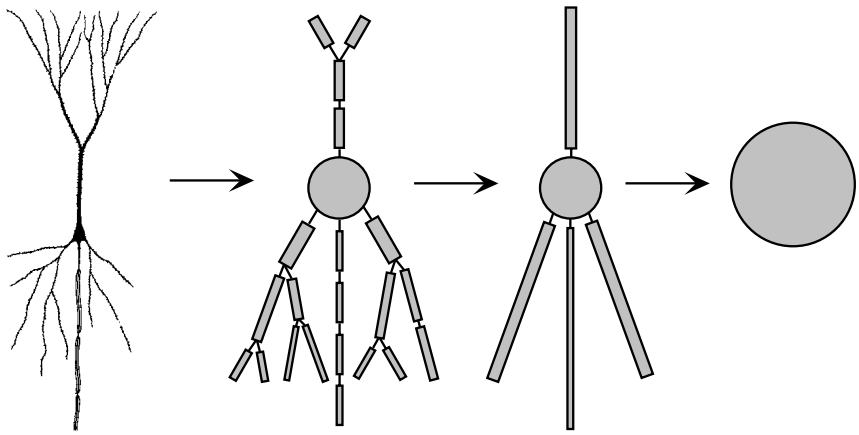

Figure 6.15 A sequence of approximations of the structure of a neuron. The neuron is represented by a variable number of discrete compartments, each representing a region that is described by a single membrane potential. The connectors between compartments represent resistive couplings. The simplest description is the single-compartment model furthest to the right.

three such terms, corresponding to coupling of the branching node to the first compartment in each of the daughter branches.

The constant $g_{\mu,\mu'}$ that determines the resistive coupling from neighboring compartment μ' to compartment μ is determined by computing the current that flows from one compartment to its neighbor due to Ohm's law. For simplicity, we begin by computing the coupling between two compartments that have the same length L and radius a. Using the results of chapter 5, the resistance between two such compartments, measured from their centers, is the intracellular resistivity, $r_{\rm L}$ times the distance between the compartment centers divided by the cross-sectional area, $r_{\rm L}L/(\pi a^2)$. The total current flowing from compartment $\mu+1$ to compartment μ is then $\pi a^2(V_{\mu+1}-V_\mu)/r_{\rm L}L$. Equation 6.29 for the potential within a compartment μ refers to currents per unit area of membrane. Thus, we must divide the total current from compartment μ' by the surface area of compartment μ, $2\pi aL$, and we find that $g_{\mu,\mu'} = a/(2r_{\rm L}L^2)$.

The value of $g_{\mu,\mu'}$ is given by a more complex expression if the two neighboring compartments have different lengths or radii. This can occur when a tapering cable is approximated by a sequence of cylindrical compartments, or at a branch point where a single compartment connects with two other compartments, as in figure 6.16. In either case, suppose that compartment μ has length L_μ and radius a_μ, and compartment μ' has length $L_{\mu'}$ and radius $a_{\mu'}$. The resistance between these two compartments is the sum of the two resistances from the middle of each compartment to the junction between them, $r_{\rm L}L_\mu/(2\pi a_\mu^2) + r_{\rm L}L_{\mu'}/(2\pi a_{\mu'}^2)$. To compute $g_{\mu,\mu'}$ we invert this expression and divide the result by the total surface area of

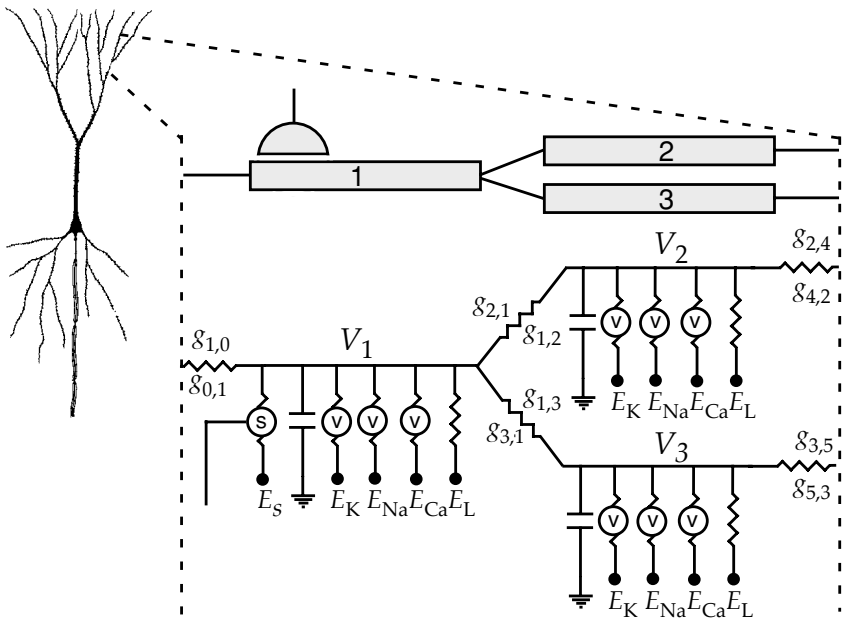

Figure 6.16 A multi-compartment model of a neuron. The expanded region shows three compartments at a branch point where a single cable splits into two. Each compartment has membrane and synaptic conductances, as indicated by the equivalent electrical circuit, and the compartments are coupled together by resistors. Although a single resistor symbol is drawn, note that $g_{\mu,\mu'}$ is not necessarily equal to $g_{\mu',\mu}$.

compartment μ, $2\pi a_\mu L_\mu$, which gives

$$g_{\mu,\mu'} = \frac{a_\mu a_{\mu'}^2}{r_L L_\mu (L_\mu a_{\mu'}^2 + L_{\mu'} a_\mu^2)}. \tag{6.30}$$

Equations 6.29 for all of the compartments of a model determine the membrane potential throughout the neuron with a spatial resolution given by the compartment size. An efficient method for integrating the coupled multi-compartment equations is discussed in appendix B. Using this scheme, models can be integrated numerically with excellent efficiency, even those involving large numbers of compartments. Such integration schemes are built into neuron simulation software packages such as Neuron and Genesis.

Action-Potential Propagation Along an Unmyelinated Axon

As an example of multi-compartment modeling, we simulate the propagation of an action potential along an unmyelinated axon. In this model, each compartment has the same membrane conductances as the single-compartment Hodgkin-Huxley model discussed in chapter 5. The different compartments are joined together in a single nonbranching cable

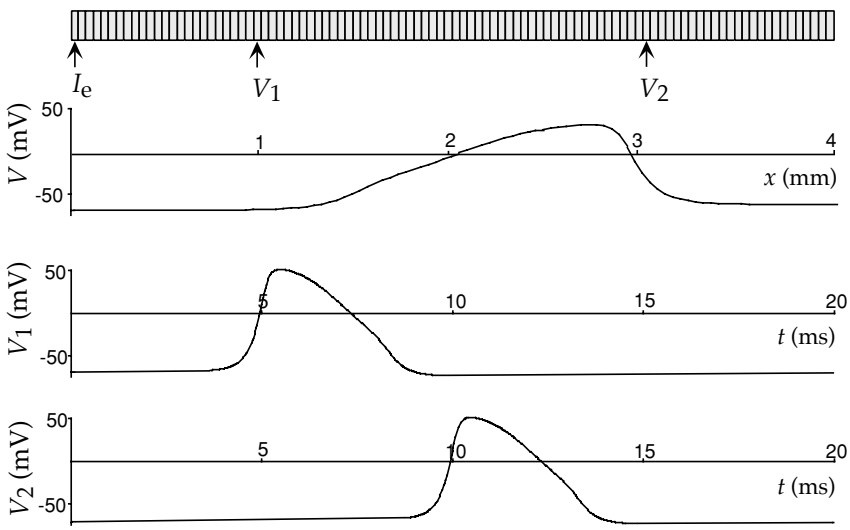

Figure 6.17 Propagation of an action potential along a multi-compartment model axon. The upper panel shows the multi-compartment representation of the axon with 100 compartments. The axon segment shown is 4 mm long and has a radius of 1 μm. An electrode current sufficient to initiate action potentials is injected at the point marked I_e. The panel beneath this shows the membrane potential as a function of position along the axon, at $t = 9.75$ ms. The spatial position in this panel is aligned with the axon depicted above it. The action potential is moving to the right. The bottom two panels show the membrane potential as a function of time at the two locations denoted by the arrows and symbols V_1 and V_2 in the upper panel.

representing a length of axon. Figure 6.17 shows an action-potential propagating along an axon modeled in this way. The action potential extends over more than 1 mm of axon and travels about 2 mm in 5 ms, for a speed of 0.4 m/s.

orthodromic and antidromic propagation

Although action potentials typically move along axons in a direction outward from the soma (called orthodromic propagation), the basic process of action-potential propagation does not favor one direction over the other. Propagation in the reverse direction, called antidromic propagation, is possible under certain stimulation conditions. For example, if an axon is stimulated in the middle of its length, action potentials will propagate in both directions away from the point of stimulation. Once an action potential starts moving along an axon, it does not generate a second action potential moving in the opposite direction because of refractory effects. The region in front of a moving action potential is ready to generate a spike as soon as enough current moves longitudinally down the axon from the region currently spiking to charge the next region up to spiking threshold. However, Na^+ conductances in the region just behind the moving action potential are still partially inactivated, so this region cannot generate another spike until after a recovery period. By the time the trailing region has recovered, the action potential has moved too far away to generate a second spike.

Refractoriness following spiking has a number of other consequences for action-potential propagation. Two action potentials moving in opposite directions that collide annihilate one another because they cannot pass through each other's trailing refractory regions. Refractoriness also keeps action potentials from reflecting off the ends of axon cables, which avoids the impedance matching needed to prevent reflection from the ends of ordinary electrical cables.

The propagation velocity for an action potential along an unmyelinated axon is proportional to the ratio of the electrotonic length constant to the membrane time constant, $\lambda/\tau_m = (a/(2c_m^2 r_L r_m))^{1/2}$. This is proportional to the square root of the axon radius. The square-root dependence of the propagation speed on the axon radius means that thick axons are required to achieve high action-potential propagation speeds, and the squid giant axon is an extreme example. Action-potential propagation can also be sped up by covering the axon with an insulating myelin wrapping, as we discuss next.

Action-Potential Propagation Along a Myelinated Axon

Many axons in vertebrates are covered with an insulating sheath of myelin except at gaps, called the nodes of Ranvier, where there is a high density of fast voltage-dependent Na^+ channels (see figure 6.18A). The myelin sheath consists of many layers of glial cell membrane wrapped around the axon. This gives the myelinated region of the axon a very high membrane resistance and a small membrane capacitance. This results in what is called saltatory propagation, in which membrane potential depolarization is transferred passively down the myelin-covered sections of the axon, and action potentials are actively regenerated at the nodes of Ranvier. Figure 6.18A shows an equivalent circuit for a multi-compartment model of a myelinated axon.

saltatory propagation

We can compute the capacitance of a myelin-covered axon by treating the myelin sheath as an extremely thick cell membrane. Consider the geometry shown in the cross-sectional diagram of figure 6.18B. The myelin sheath extends from the radius a_1 of the axon core to the outer radius a_2. For calculational purposes, we can think of the myelin sheath as being made of a series of thin, concentric cylindrical shells. The capacitances of these shells combine in series to make up the full capacitance of the myelinated axon. If a single layer of cell membrane has thickness d_m and capacitance per unit area c_m, the capacitance of a cylinder of membrane of radius a, thickness Δa, and length L is $c_m 2\pi d_m L a/\Delta a$. According to the rule for capacitors in series, the inverse of the total capacitance is obtained by adding the inverses of the individual capacitances. The capacitance of a myelinated cylinder of length L and the dimensions in figure 6.18B is then obtained by taking the limit $\Delta a \to 0$ and integrating,

$$\frac{1}{C_m} = \frac{1}{c_m 2\pi d_m L}\int_{a_1}^{a_2}\frac{da}{a} = \frac{\ln(a_2/a_1)}{c_m 2\pi d_m L}. \qquad (6.31)$$

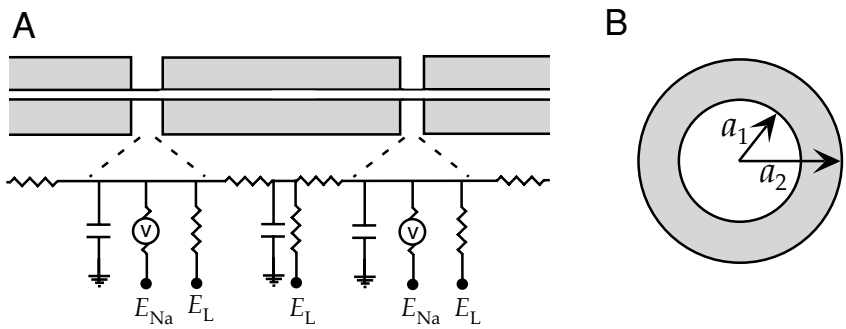

Figure 6.18 A myelinated axon. (A) The equivalent circuit for a multi-compartment representation of a myelinated axon. The myelinated segments are represented by a membrane capacitance, a longitudinal resistance, and a leakage conductance. The nodes of Ranvier also contain a voltage-dependent Na^+ conductance. (B) A cross section of a myelinated axon consisting of a central axon core of radius a_1 and a myelin sheath making the outside radius a_2.

A re-evaluation of the derivation of the linear cable equation earlier in this chapter indicates that the equation describing the membrane potential along the myelinated sections of an axon, in the limit of infinite resistance for the myelinated membrane and with $i_e = 0$, is

$$\frac{C_m}{L}\frac{\partial v}{\partial t} = \frac{\pi a_1^2}{r_L}\frac{\partial^2 v}{\partial x^2}. \tag{6.32}$$

This is equivalent to the diffusion equation, $\partial v/\partial t = D\partial^2 v/\partial x^2$, with diffusion constant $D = \pi a_1^2 L/(C_m r_L) = a_1^2 \ln(a_2/a_1)/(2c_m r_L d_m)$. It is interesting to compute the inner core radius, a_1, that maximizes this diffusion constant for a fixed outer radius a_2. Setting the derivative of D with respect to a_1 to 0 gives the optimal inner radius $a_1 = a_2 \exp(-1/2)$ or $a_1 \approx 0.6a_2$. An inner core fraction of 0.6 is typical for myelinated axons. This indicates that for a given outer radius, the thickness of myelin maximizes the diffusion constant along the myelinated axon segment.

At the optimal ratio of radii, $D = a_2^2/(4ec_m r_L d_m)$, which is proportional to the square of the axon radius. Because of the form of the diffusion equation it obeys with this value of D, v can be written as a function of x/a_2 and t. This scaling implies that the propagation velocity for a myelinated cable is proportional to a_2, that is, to the axon radius, not its square root (as in the case of an unmyelinated axon). Increasing the axon radius by a factor of 4, for example, increases the propagation speed of an unmyelinated cable only by a factor of 2, while it increases the speed for a myelinated cable fourfold.

6.5 Chapter Summary

We continued the discussion of neuron modeling that began in chapter 5 by considering models with more complete sets of conductances and techniques for incorporating neuronal morphology. We introduced A-type K^+, transient Ca^{2+}, and Ca^{2+}-dependent K^+ conductances, and noted their effect on neuronal activity. The cable equation and its linearized version were introduced to examine the effects of morphology on membrane potentials. Finally, multi-compartment models were presented and used to discuss propagation of action potentials along unmyelinated and myelinated axons.

6.6 Appendices

A: Gating Functions for Conductance-Based Models

Connor-Stevens Model

The rate functions used for the gating variables n, m, and h of the Connor-Stevens model, in units of $1/\text{ms}$ with V in units of mV, are

$$\begin{aligned} \alpha_m &= \frac{0.38(V+29.7)}{1-\exp(-0.1(V+29.7))} & \beta_m &= 15.2\exp(-0.0556(V+54.7)) \\ \alpha_h &= 0.266\exp(-0.05(V+48)) & \beta_h &= 3.8/(1+\exp(-0.1(V+18))) \\ \alpha_n &= \frac{0.02(V+45.7)}{1-\exp(-0.1(V+45.7))} & \beta_n &= 0.25\exp(-0.0125(V+55.7))\,. \end{aligned} \tag{6.33}$$

The A-current is described directly in terms of the asymptotic values and τ functions for its gating variables (with τ_a and τ_b in units of ms and V in units of mV),

$$a_\infty = \left(\frac{0.0761\exp(0.0314(V+94.22))}{1+\exp(0.0346(V+1.17))}\right)^{1/3} \tag{6.34}$$

$$\tau_a = 0.3632 + 1.158/(1+\exp(0.0497(V+55.96))) \tag{6.35}$$

$$b_\infty = \left(\frac{1}{1+\exp(0.0688(V+53.3))}\right)^4 \tag{6.36}$$

and

$$\tau_b = 1.24 + 2.678/(1+\exp(0.0624(V+50)))\,. \tag{6.37}$$

Transient Ca^{2+} Conductance

The gating functions used for the variables M and H in the transient Ca^{2+} conductance model we discussed, with V in units of mV and τ_M and τ_H in ms, are

$$M_\infty = \frac{1}{1 + \exp\left(-(V+57)/6.2\right)} \tag{6.38}$$

$$H_\infty = \frac{1}{1 + \exp\left((V+81)/4\right)} \tag{6.39}$$

$$\tau_M = 0.612 + \left(\exp\left(-(V+132)/16.7\right) + \exp\left((V+16.8)/18.2\right)\right)^{-1} \tag{6.40}$$

and

$$\tau_H = \begin{cases} \exp\left((V+467)/66.6\right) & \text{if } V < -80 \text{ mV} \\ 28 + \exp\left(-(V+22)/10.5\right) & \text{if } V \geq -80 \text{ mV}. \end{cases} \tag{6.41}$$

Ca^{2+}-dependent K^+ Conductance

The gating functions used for the Ca^{2+}-dependent K^+ conductance we discussed, with V in units of mV and τ_c in ms, are

$$c_\infty = \left(\frac{[Ca^{2+}]}{[Ca^{2+}] + 3\mu M}\right) \frac{1}{1 + \exp(-(V+28.3)/12.6)} \tag{6.42}$$

and

$$\tau_c = 90.3 - \frac{75.1}{1 + \exp(-(V+46)/22.7)}\,. \tag{6.43}$$

B: Integrating Multi-compartment Models

Multi-compartment models are defined by a coupled set of differential equations (equation 6.29), one for each compartment. There are also gating variables for each compartment, but these involve only the membrane potential (and possibly Ca^{2+} concentration) within that compartment, and integrating their equations can be handled as in the single-compartment case using the approach discussed in appendix B of chapter 5. Integrating the membrane potentials for the different compartments is more complex because they are coupled to each other.

Equation 6.29, for the membrane potential within compartment μ, can be written in the form

$$\frac{dV_\mu}{dt} = A_\mu V_{\mu-1} + B_\mu V_\mu + C_\mu V_{\mu+1} + D_\mu\,, \tag{6.44}$$

where

$$A_\mu = c_m^{-1} g_{\mu,\mu-1}\,, \quad B_\mu = -c_m^{-1}\Big(\sum_i g_i^\mu + g_{\mu,\mu+1} + g_{\mu,\mu-1}\Big)\,,$$
$$C_\mu = c_m^{-1} g_{\mu,\mu+1}\,, \quad D_\mu = c_m^{-1}\Big(\sum_i g_i^\mu E_i + I_e^\mu / A_\mu\Big)\,. \tag{6.45}$$

Note that the gating variables and other parameters have been absorbed into the values of A_μ, B_μ, C_μ, and D_μ in this equation. Equation 6.44, with μ running over all of the compartments of the model, generates a set of coupled differential equations. Because of the coupling between compartments, we cannot use the method discussed in appendix A of chapter 5 to integrate these equations. Instead, we present another method that shares some of the positive features of that approach. The Runge-Kutta method, which is a standard numerical integrator, is poorly suited for this application and is likely to run orders of magnitude slower than the method described below.

Two of the most important features of an integration method are accuracy and stability. Accuracy refers to how closely numerical finite-difference methods reproduce the exact solution of a differential equation as a function of the integration step size Δt. Stability refers to what happens when Δt is chosen to be excessively large and the method starts to become inaccurate. A stable integration method will degrade smoothly as Δt is increased, producing results of steadily decreasing accuracy. An unstable method, on the other hand, will at some point display a sudden transition and generate wildly inaccurate results. Given the tendency of impatient modelers to push the limits on Δt, it is highly desirable to have a method that is stable.

Defining

$$V_\mu(t + \Delta t) = V_\mu(t) + \Delta V_\mu\,, \tag{6.46}$$

the finite difference form of equation 6.44 gives the update rule

$$\Delta V_\mu = \big(A_\mu V_{\mu-1}(t) + B_\mu V_\mu(t) + C_\mu V_{\mu+1}(t) + D_\mu\big)\,\Delta t\,, \tag{6.47}$$

which is how ΔV_μ is computed using the so-called Euler method. This method is both inaccurate and unstable. The stability of the method can be improved dramatically by evaluating the membrane potentials on the right side of equation 6.47 not at time t, but at a later time $t + z\Delta t$, so that

$$\Delta V_\mu = \big(A_\mu V_{\mu-1}(t + z\Delta t) + B_\mu V_\mu(t + z\Delta t) + C_\mu V_{\mu+1}(t + z\Delta t) + D_\mu\big)\,\Delta t\,. \tag{6.48}$$

Two such methods are predominantly used, the reverse Euler method, for which $z = 1$, and the Crank-Nicholson method with $z = 0.5$. The reverse Euler method is the more stable of the two and the Crank-Nicholson is the more accurate. In either case, ΔV_μ is determined from equation 6.48. These methods are called implicit because equation 6.48 must be solved

to determine ΔV_μ. To do this, we write $V_\mu(t + z\Delta t) \approx V_\mu(t) + z\Delta V_\mu$ and likewise for $V_{\mu\pm1}$. Substituting this into equation 6.48 gives

$$\Delta V_\mu = a_\mu \Delta V_{\mu-1} + b_\mu \Delta V_\mu + c_\mu \Delta V_{\mu+1} + d_\mu \,, \tag{6.49}$$

where

$$\begin{aligned} a_\mu &= A_\mu z\Delta t \,, \quad b_\mu = B_\mu z\Delta t \,, \quad c_\mu = C_\mu z\Delta t \,, \\ d_\mu &= (D_\mu + A_\mu V_{\mu-1}(t) + B_\mu V_\mu(t) + C_\mu V_{\mu+1}(t))\Delta t \,. \end{aligned} \tag{6.50}$$

Equation 6.49 for all μ values provides a set of coupled linear equations for the quantities ΔV_μ. An efficient method exists for solving these equations (Hines, 1984; Tuckwell, 1988). We illustrate the method for a single, nonbranching cable that begins at compartment $\mu = 1$, so that $a_1 = 0$, and ends at compartment $\mu = N$, so $c_N = 0$. The method consists of solving equation 6.49 for ΔV_μ in terms of $\Delta V_{\mu+1}$ sequentially, starting at one end of the cable and proceeding to the other end. For example, if we start the procedure at compartment 1, ΔV_1 can be expressed as

$$\Delta V_1 = \frac{c_1 \Delta V_2 + d_1}{1 - b_1} . \tag{6.51}$$

Substituting this into the equation 6.49 for $\mu = 2$ gives

$$\Delta V_2 = b_2' \Delta V_2 + c_2 \Delta V_3 + d_2' \,, \tag{6.52}$$

where $b_2' = b_2 + a_2 c_1/(1 - b_1)$ and $d_2' = d_2 + a_2 d_1/(1 - b_1)$. We now repeat the procedure going down the cable. At each stage, we solve for $\Delta V_{\mu-1}$ in terms of ΔV_μ, finding

$$\Delta V_{\mu-1} = \frac{c_{\mu-1} \Delta V_\mu + d_{\mu-1}'}{1 - b_{\mu-1}'} \,, \tag{6.53}$$

where

$$b_{\mu+1}' = b_{\mu+1} + \frac{a_{\mu+1} c_\mu}{1 - b_\mu'} \tag{6.54}$$

and

$$d_{\mu+1}' = d_{\mu+1} + \frac{a_{\mu+1} d_\mu'}{1 - b_\mu'} \,. \tag{6.55}$$

Finally, when we get to the end of the cable, we can solve for

$$\Delta V_N = \frac{d_N'}{1 - b_N'} \tag{6.56}$$

because $c_N = 0$.

The procedure for computing all the ΔV_μ is the following. Define $b_1' = b_1$ and $d_1' = d_1$ and iterate equations 6.54 and 6.55 down the length of the

cable to define all the b' and d' parameters. Then solve for ΔV_N from equation 6.56 and iterate back up the cable, solving for the ΔV's using 6.53. This process takes only $2N$ steps.

We leave the extension of this method to the case of a branched cable as an exercise for the reader. The general procedure is similar to the one we presented for a nonbranching cable. The equations are solved by starting at the ends of the branches and moving in toward their branching node, then continuing on as for a nonbranching cable, and finally reversing direction and completing the solution moving in the opposite direction along the cable and its branches.

6.7 Annotated Bibliography

Many of the references for chapter 5 apply to this chapter as well, including **Jack et al. (1975)**, **Tuckwell (1988)**, **Johnston & Wu (1995)**, **Koch & Segev (1998)**, **Koch (1998)**, **Hille (1992)**, and **Mascagni & Sherman (1998)**. **Rall (1977)** describes cable theory, the equivalent cable model of dendritic trees, and the 3/2 law. The solution of equation 6.21 can be constructed using the set of rules for solving the linear cable equation on arbitrary trees found in Abbott (1992; see also Abbott et al., 1991). **Marder & Calabrese (1996)** reviews neuromodulation.

Two freely available software packages for detailed neuronal modeling are in wide use, `Neuron` (see Hines & Carnevale, 1997) and `Genesis` (see Bower & Beeman, 1998). These are available at `http://www.neuron.yale.edu` and `http://genesis.bbb.caltech.edu/GENESIS/genesis.html`.

7 Network Models

7.1 Introduction

Extensive synaptic connectivity is a hallmark of neural circuitry. For example, a typical neuron in the mammalian neocortex receives thousands of synaptic inputs. Network models allow us to explore the computational potential of such connectivity, using both analysis and simulations. As illustrations, we study in this chapter how networks can perform the following tasks: coordinate transformations needed in visually guided reaching, selective amplification leading to models of simple and complex cells in primary visual cortex, integration as a model of short-term memory, noise reduction, input selection, gain modulation, and associative memory. Networks that undergo oscillations are also analyzed, with application to the olfactory bulb. Finally, we discuss network models based on stochastic rather than deterministic dynamics, using the Boltzmann machine as an example.

cortical columns

feedforward, recurrent, and top-down connections

Neocortical circuits are a major focus of our discussion. In the neocortex, which forms the convoluted outer surface of the (for example) human brain, neurons lie in six vertical layers highly coupled within cylindrical columns. Such columns have been suggested as basic functional units, and stereotypical patterns of connections both within a column and between columns are repeated across cortex. There are three main classes of interconnections within cortex, and in other areas of the brain as well. Feedforward connections bring input to a given region from another region located at an earlier stage along a particular processing pathway. Recurrent synapses interconnect neurons within a particular region that are considered to be at the same stage along the processing pathway. These may include connections within a cortical column as well as connections between both nearby and distant cortical columns within a region. Top-down connections carry signals back from areas located at later stages. These definitions depend on the how the region being studied is specified and on the hierarchical assignment of regions along a pathway. In general, neurons within a given region send top-down projections back to the areas from which they receive feedforward input, and receive top-down input from the areas to which they project feedforward output. The numbers, though not necessarily the strengths, of feedforward and top-down